Investigating immune cell infiltrates in canine (sub)cutaneous soft tissue sarcoma and cell death in canine cutaneous histiocytoma

Thesis submitted in fulfilment of the requirements of the University of Glasgow for the degree of Master in Veterinary Medicine

By

Samuel Kalpers DVM, MRCVS, ECVP Diplomate

School of Veterinary Medicine, College of Medical, Veterinary and Life Science

April 2026

Abstract

Investigation of the tumour microenvironment is scarce in canine cutaneous and subcutaneous soft tissue sarcomas (STSs) and previously has not been carried out with a focus on the spatial distribution (central tumour versus infiltrating margin) of inflammatory cells infiltrating the tumour. In canine cutaneous histiocytoma (CCH), investigations of the tumour microenvironment have not yet allowed to fully elucidate the mechanisms leading to regression. This research project investigated the tumour microenvironment of these two tumours, at the same time examining the utility of the image analysis program QuPath to support the investigations.

In the first part of this study, the extent and subsets of infiltrating immune cells, including their spatial distribution, of 15 grade I and 15 grade III STSs was investigated by immunohistochemistry (IHC) with antibodies against CD3, CD20, CD204, CD206, Granzyme B and FOXP3. When examining all 30 STSs combined, the expression of CD3, CD20, FOXP3 and granzyme B was statistically significantly ($p<0.05$) higher in the invasive margin compared to central tumour areas, however there were no statistical differences when comparing the immune cell infiltrates in invasive margin and central tumour between grade I and III tumours. Dogs with a better clinical outcome exhibited higher CD20, CD3, Granzyme B, FOXP3 and CD204 immunolabelling in the invasive margin when compared to dogs with a worse clinical outcome, warranting further research on the immune environment and clinical outcome of STSs, in particular with a focus on the invasive margin of these tumours.

In the second part of the study, immune infiltrates and markers of cell death were investigated in 30 CCH cases at different stages of regression by IHC with antibodies against CD3, CD204, HMGB1 and Activated Caspase 3. CD3, CD204 and Activated Caspase 3 increased significantly ($p<0.05$) with regression whereas HMGB1 labelling was not significantly modified. Therefore, apoptosis appears to be the main cell death pathway involved in CCH regression. However, bearing in mind the robust histiocytic inflammatory response incited in the regression of CCH, further investigations in the exact mechanisms of cell death continue to be warranted which may also help elucidate the mechanisms underlying regression.

Overall, automated image analysis, using QuPath, allowed to gather quantitative (and objective) data one whole scanned slides, which in turn was comparable to results from previously published data acquired by manual counting of cells, in turn validating this approach. However, the training of QuPath is labour and time intensive and necessitates supervision of attentive and trained operators. Furthermore, the algorithms generated are anticipated to only be able to be applied on the present datasets since staining parameters are expected to vary in differing IHC protocols and scanning settings. Therefore, whilst automated image analysis can provide highly objective data, possibilities and drawbacks need to be taken into account before proceeding with the element of machine learning/training.

Table of Contents

List of Tables

List of Figures

Acknowledgments

I would like to thank my supervisor, Angie Rupp, for her guidance and help without whom this thesis would not have been possible. Thanks go also to Francesco Marchesi, Kate Ings, Mark Dagleish, Alex Gray and Pamela Johnston for their support throughout my residency.

Special thanks go to Rheinallt Jones for his kindness, invaluable support and mentoring regarding QuPath and statistical analysis.

Special thanks go to Katie McNaught for her help gathering clinical data.

Thanks to the histopathology lab team, Lynn Stevenson, Lynn Oxford, Lewis Kidd and Frazer Bell for their amazing technical work, expertise and guidance throughout this journey.

Thanks to the anatomic pathology residents, Amy, Elisa and Enni for their support and friendship.

Thanks to the Veterinary Small Grants Fund for funding the work in this thesis.

Thanks to my wonderful partner, Chloé, for her support, patience and love.

List of Abbreviations

APC : Antigen presenting cells

CAFs : Cancer Associated Fibroblasts

CCH : Canine cutaneous histiocytoma

CD204 : Class 1 macrophage scavenger receptor

CD206 : Macrophage mannose receptor 1

CT : Central tumour

CTL : Cytotoxic T lymphocyte

CTLA : Cytotoxic T-lymphocyte associated protein

DAMP : Damage associated molecular pattern

ECM : Extracellular matrix

FFPE: Formalin-fixed paraffin embedded

FOXP3: Forkhead box P3

H&E: Haematoxylin and Eosin

HMGB1: High-mobility group box I

IC: Immune cell

ICD: Immunogenic cell death

IHC: Immunohistochemistry

IM: Invasive margin

IQR: Interquartile range

PNST: Peripheral nerve sheath tumour

PWT: Perivascular wall tumour

MHCI: Major Histocompatibility Complex I

MHCII: Major Histocompatibility Complex II

NCCD: Nomenclature Committee on Cell Death

N/C ratio: Nuclear to cytoplasmic ratio

NK cells: Natural Killer cells

RAGE: Receptor for advanced glycation end products

SAH: Small Animal Hospital

STS: Soft tissue sarcoma

TAN: Tumour associated neutrophils

TE: Tumour environment

Th: T helper lymphocyte

TIL: Tumour infiltrating lymphocyte

TME: Tumour microenvironment

Tregs: Regulatory T lymphocyte

TUNEL: Terminal deoxynucleotidyl transferase-mediated dUTP nick-end labelling

VDS: Veterinary Diagnostic Service

1 Introduction

1.1 Tumour microenvironment

1.1.1 General background

The first principles of tumour microenvironment (TME) were laid in the 19th century by Virchow, who first theorized a link between inflammation and oncogenesis (Maman and Witz 2018, Schmidt and Weber 2006). In the same century, Paget formulated the “seed and soil” theory after noticing some organs are more prone to be affected by metastasis regardless of their relative blood flow (Maman and Witz 2018, Paget 1989). However, the first published reports mentioning TME date to 1975 following a study in rats with 20-methylcholanthrene-induced sarcoma. The authors, investigating circulating tumour antigens and antibodies specific to these antigens, concluded that tumour antigens can interfere with the immune cell function and their ability to elicit an immune response directed against the tumour (Thomson 1975). Later in the same year, Preisler et al. concluded by doing in vitro experiments on Friend leukaemia cells that the TME had a role in the differentiation of leukemic cells into granulocytic or erythrocytic phenotype (Preisler et al. 1975). Since then, the TME has become a central research topic in oncology and immuno-oncology with the ambition to harness this phenomenon for novel therapies, in turn broadening the scope of the therapeutic arsenal to treat cancer (Balkwill et al. 2012, Boxberg et al. 2019, Han et al. 2024, Jin and Jin 2020, Martinez and Moon 2019). In addition, the study of TME has helped to improve our understanding of tumour biology, including the relationship between neoplastic cells and the patient. This knowledge has also been applied to select biomarkers to estimate tumour prognosis and also the response to therapy (Jain 2013).

There is no clear definition of the TME, as it can refer to a wide scope of concepts (Laplane et al. 2018). For some authors, the TME represents the interactions between neoplastic and non-neoplastic cells (Balkwill et al. 2012). To others, it represents all the elements that interact with the tumour cells, both at the vicinity of the tumour and also at more distant sites such as the gut, where it includes the microbiota, or remote immune organs such as the bone marrow and other components of the haematopoietic system (Laplane et al.

2018). Nevertheless, the TME is considered to be dynamic and can lead to altered phenotypes of the extra-cellular matrix (ECM), neoplastic and non-neoplastic cells and thus regulate survival, propagation and progression of tumours (Anderson and Simon 2020, Laplane et al. 2018, Maman and Witz 2018).

In general, within tumours, the three main constituents of the TME are the cellular component, the cytokines and chemokines secreted by these cells, and the non-cellular components present in an ECM (Maman and Witz 2018). The cellular component of the TME is represented by the neoplastic cells, immune cells, endothelial cells, pericytes, fibroblasts, and adipocytes, whereby the immune cell component specifically includes tumour infiltrating lymphocytes (TILs), tumour associated macrophages (TAMs), dendritic cells, myeloid-derived suppressor cells and neutrophils. The non-cellular and cellular components are interdependent and are implicated in a crosstalk leading to complex network of positive and negative feedback loops which ultimately give the TME a promoting or suppressing effect on the neoplastic cells (Anderson and Simon 2020, Balkwill et al. 2012, Mao et al. 2021). In addition, the TME appears to be specific to tumour types and depending on the tumour type, the presence of a specific cell type or biomarker may represent a positive or negative prognostic factor (Balkwill et al. 2012).

1.1.2 Tumour infiltrating lymphocytes

Investigation of TILs has become an active subject in immuno-oncology, especially considering the advent of novel therapies such as immune checkpoint inhibitors (Giuliano et al. 2024, Stanton and Disis 2016). As a result, the International Immuno-Oncology Biomarkers Working Group, working on tumours of humans, has published recommendations for the assessment of TILs in the TME both for standard (Haematoxylin & Eosin) and immunohistochemical (IHC) stains. In addition, they recommend the use of different compartments to assess the TME, such as areas located in the centre of the tumours and areas located at the invasive margin of the tumours (Hendry et al. 2017a, Hendry et al. 2017b). In Veterinary onco-pathology, these guidelines so far have only been applied in canine mammary tumours (Muscatello et al. 2022).

1.1.2.1 Types of lymphocytes

Different types and subtypes of lymphocytes exist, each exerting different immunological functions and are a part of the adaptive immune response. The two major categories of lymphocytes are B and T cells (Hendry et al. 2017b, Snyder 2017). The T cell category includes CD4+ and CD8+ cells, with CD4+ T cells subdivided in a broad range of different types of T helper cells and T regulator lymphocytes (Tregs) (Hendry et al. 2017b, Snyder 2017), and CD8+ T cells representing cytotoxic T lymphocytes (Farhood et al. 2019). The main function of B cells is to produce antibodies whereas the T cell function varies depending on the subtype (Snyder 2017).

The T helper cells, for which Th1 and Th2 are the main subtypes, modulate the immune system through the expression and release of specific cytokines, which in turn drives the appropriate response towards a particular noxious stimulus (Lang et al. 2024, Ruterbusch et al. 2020). In the context of tumour immunity, a Th1 driven immune response is generally associated with a more favourable outcome compared to a Th2 driven immune response (Hendry et al. 2017b, Stanton and Disis 2016). Tregs, on the other hand, typically have an anti-inflammatory and immunosuppressive function which helps regulate the immune system, for example preventing autoimmune diseases. Within tumours, increased numbers of Tregs are more often associated with malignancy and poor prognosis (Biller et al. 2007, Fortuna et al. 2016).

Cytotoxic T lymphocytes (CTLs), are able to recognize abnormal proteins expressed on other cells and can induce programmed cell death either by releasing cytotoxic granules containing granzyme B and perforin, or by interacting directly with the target cell through binding of their Fas ligand with the Fas protein on the target cell membrane, leading to apoptosis (Farhood et al. 2019). Similar to CTLs, natural killer cells (NK cells), a cytotoxic effector cell, however of the innate immunity, can also induce programmed cell death through the release of cytotoxic granules, containing granzyme B and perforin, and Fas ligand interaction (Prager et al. 2019). Contrary to CTLs, NK cells however do not express surface CD3 and are activated early in the immune response (Snyder 2017).

Although this is not true for all tumours, it appears that in most cases the activity of Th1 cells, NK cells and CTLs is associated with an antitumorigenic effect (Stanton and Disis 2016), whereas the presence of Th2 cells and Tregs is associated with inhibition of an appropriate immune response against tumour cells (Biller et al. 2007, Stanton and Disis 2016). Furthermore, increased numbers of Th2 cells and Tregs are associated with malignancy and represent a negative prognostic factor (Biller et al. 2007, Stanton and Disis 2016).

Immunohistochemistry can be applied to differentiate lymphocyte subtypes. However, on formalin-fixed paraffin embedded tissue (FFPE), the identification of lymphocyte subtypes can be challenging as a broader range of commercially available markers only work on frozen sections or by flow cytometry when consulting the datasheets of the manufacturers. In dogs, the markers most commonly used to highlight B cells are antibodies against CD20 (Jubala et al. 2005), CD79α (Stonehewer et al. 1998) and PAX5 (Willmann et al. 2009). A reliable T cell antigen is CD3 (Ferrer et al. 1992) and investigation of the presence of CTLs can be achieved with anti-CD8 antibody (Nururrozi et al. 2024). Unfortunately, however, a commercially available marker for CD8 in FFPE is lacking for canine tissue. Therefore, and alternatively, a marker against granzyme B often is used although it will – as detailed above - also label NK cells (Lane et al. 2012). Antibodies against forkhead box P3 (FOXP3), a transcription factor specific to Tregs, have been demonstrated to successfully label Tregs in dogs (Belluco et al. 2020, Boozer et al. 2012, Fortuna et al. 2016, Maeda et al. 2016). Finally, the distinction between Th1 and Th2 subtypes in dogs can only be achieved by flow cytometry (Lang et al. 2024) as reliable IHC markers for FFPE tissues are yet to be investigated. Interestingly, in humans, the use of antibodies against T-bet and GATA-3 to label Th1 and Th2 cells, respectively, in FFPE tissues has recently been reported (Satomi et al. 2025).

1.1.3 Tumour associated macrophages

1.1.3.1 Types of macrophages

Similar to the Th1/Th2 differentiation of lymphocytes, macrophages can also exhibit different phenotypes, broadly classified as polarized towards a M1 or M2 phenotype. In general, M1 macrophages are reported to be proinflammatory and

antitumorigenic, whereas M2 macrophages display an anti-inflammatory and protumorigenic effect (Kerboeuf et al. 2024, Liu et al. 2021, Zhang et al. 2021). A broad range of IHC markers is used in humans. M1 macrophages can be investigated with antibodies against CD83, CD80, CD40, inducible nitric oxide synthase (Lopez-Janeiro et al. 2020), RBP-J, pSTAT1 (Barros et al. 2013), HLA-DR and CD197 (Liu et al. 2021), whilst antibodies against CMAF (Barros et al. 2013), CD204 (Lopez-Janeiro et al. 2020), CD163, CD206, and CCL2 label M2 macrophages (Liu et al. 2021). Some authors recommend using more than one marker to identify polarization (Barros et al. 2013).

However, the proteins expressed by human M1 and M2 macrophages are different from the proteins expressed in canine M1 and M2 macrophages (Heinrich et al. 2017) and the use of appropriate markers to examine macrophage subsets has generated spirited debate amongst pathologists (Belluco 2018, Sur 2018). Currently, anti-Iba1 antibodies are considered to represent a robust marker of all cells of the monocytic/histiocytic lineage, which includes macrophages, dendritic cells, Langerhans cells and microglial cells (Ahmed et al. 2007, Bertola et al. 2024, Ito et al. 1998). A more specific marker for resident and infiltrating macrophages is the class A macrophage scavenger receptor (CD204), which, according to the literature does not label regular canine dendritic and Langerhans cells or histiocytoma cells (Moore 2014, Moore 2023). Currently, antibodies against the macrophage mannose receptor 1 (CD206) are the only markers used consensually for M2 macrophages (Belluco et al. 2020, Heinrich et al. 2017, Kerboeuf et al. 2024, Monteiro et al. 2018); there is a lack of a specific M1 macrophage markers (Heinrich et al. 2017).

1.2 Cell death

1.2.1 Types of cell death

According to the latest publication by the Nomenclature Committee on Cell Death (NCCD), cell death is defined as the “irreversible degeneration of vital cellular functions (notably ATP production and preservation of redox homeostasis) culminating in the loss of cellular integrity (permanent plasma membrane permeabilization or cellular fragmentation)” (Galluzzi et al. 2018). Morphologically, pathologists distinguish (only) two types of cell death on

routine histological sections; these are referred to as necrosis or apoptosis. Necrotic cells exhibit pyknotic over karyorrhectic to karyolytic nuclei and a (commonly expanded) eosinophilic cytoplasm, whereas apoptotic cells are characterized by the shrinkage of the hypereosinophilic cell and fragmentation of the nucleus into small apoptotic bodies. Necrosis typically results in disruption of the cytoplasmic membrane and release of intracellular material into the extracellular space, in turn eliciting an inflammatory reaction, whereas apoptosis does not generally induce an inflammatory response (Miller and Zachary 2017). However, more recent work suggest that the binary view of necrosis versus apoptosis should be abandoned when investigating cell death pathways as necrosis is an “umbrella term” which does not refer to a specific mechanism of cell death (Santagostino et al. 2021).

Cell death has been an intense subject of investigation over the past decades, the body of knowledge on which is continually expanding. A discussion of all the mechanisms of cell death is beyond the scope of this work, however, comprehensive reviews in this evolving field of research are published regularly (Newton et al. 2024, Santagostino et al. 2021, Yuan and Ofengeim 2024).

In general, cell death can be defined as “regulated” or “not regulated” (Galluzzi et al. 2018, Newton et al. 2024, Santagostino et al. 2021, Yuan and Ofengeim 2024) and the NCCD now recognizes 12 major mechanisms of regulated cell death (Galluzzi et al. 2018). Amongst the numerous types of regulated cell death, apoptosis was the first to be defined as such (Kerr et al. 1972) and has been studied in depth. On FFPE tissues, Active (or cleaved) Caspase 3, which represents an executioner caspase of apoptosis, has proven to represent a robust IHC target for apoptosis (Krajewska et al. 1997, Pelletier et al. 2000, Santagostino et al. 2021) in addition to the terminal deoxynucleotidyl transferase-mediated dUTP nick end labelling (TUNEL) assay which identifies DNA fragmentation secondary to cell death (Galluzzi et al. 2009, Pelletier et al. 2000, Santagostino et al. 2021). Another type of regulated cell death of interest in cancer biology is immunogenic cell death (ICD), defined as “a form of regulated cell death that is sufficient to activate an adaptive immune response in immunocompetent hosts” by the NCCD (Galluzzi et al. 2018). It is characterized by the release of damage-associated molecular patterns (DAMPs) by cells undergoing cell death. The DAMPs are recognized by pattern recognition

receptors located on innate and adaptive immune cells, in turn resulting in an immune response (Galluzzi et al. 2018). The NCCD lists 6 DAMPs which are reported to elicit an immune response, namely calreticulin, ATP, high-mobility group box I (HMGB1), type I interferon, cancer cell-derived nucleic acids and annexin A1 (Galluzzi et al. 2018). Of these, HMGB1 has been used successfully as an IHC target for ICD on FFPE samples in humans (Schlueter et al. 2005) and dogs (Sterenczak et al. 2011). High-mobility group box I is a structural protein of the chromatin which in its physiological status is located in the nucleus and, upon cell death or immune cell activation, can translocate into the cytoplasm and extracellular space (Tang et al. 2023).

1.2.2 Cell death in the context of tumours

Interestingly, the study of cell death and tumour biology has been intrinsically linked in modern research as exemplified by the discovery of bcl-2 in a subtype of human B cell lymphoma (Pegoraro et al. 1984). It was later discovered that bcl-2, an intracellular protein, prevents apoptosis (Garcia et al. 1992) by regulating the intrinsic pathway of apoptosis (Galluzzi et al. 2018). Research has shown that malignant neoplastic cells can evade and modify homeostatic mechanisms of regulated cell death, consequently promoting neoplastic cell survival (Newton et al. 2024); these include the escape of an appropriate immune response (Singh et al. 2024). Accordingly, current therapeutic strategies in oncology are aimed at inducing types of cell death which can elicit an antineoplastic immune response, or at (re-)activating immune cells already infiltrating the tumour, such as the use of immune checkpoint inhibitors (Arimoto et al. 2024).

1.3 Canine cutaneous and subcutaneous soft tissue sarcomas

Canine cutaneous and subcutaneous soft tissue sarcomas (STSs) represent a heterogenous group of malignant mesenchymal tumours of the soft connective tissues, which originate from different cell lineages but exhibit a similar biological behaviour. Soft tissue sarcomas includes fibrosarcomas, myxosarcomas, malignant peripheral nerve sheath tumours, liposarcomas, perivascular wall tumours, pleomorphic sarcomas (also known as malignant

fibrous histiocytomas), malignant mesenchymomas and undifferentiated sarcomas (Bray 2016, Dennis et al. 2011).

Several negative prognostic factors have been determined in canine cutaneous and subcutaneous STSs. These include incomplete surgical margins (Bray et al. 2014, Ettinger et al. 2006), high grade (Dennis et al. 2011), high mitotic score, high Ki-67 labelling, high AgNOR score labelling (Ettinger et al. 2006) and evidence of activation of the Akt signalling pathway (Miyanishi et al. 2023).

Currently, veterinary pathologists routinely assess the histological grade of canine cutaneous and subcutaneous STSs by evaluating three criteria: the mitotic rate, extent of necrosis and cellular differentiation. Each criterium is assigned a score which are added together to give a total score for which a grade ranging from I to III is attributed (Dennis et al. 2011). This grading system was historically designed for human STSs and initially published in the eighties (Trojani et al. 1984). Since then, it has been demonstrated that this grading system, applied to dogs, is a relatively good predictor for metastasis and recurrence (Bray et al. 2014). On the other hand, it appears the canine grading system has only moderate inter-observer agreement, thus complicating accurate and reproducible grading amongst pathologists (Yap et al. 2017).

To date, only a small number of studies have investigated tumour immune infiltrates in canine cutaneous and subcutaneous STSs, and little is known regarding the particular lymphocyte or macrophage subsets (Avallone et al. 2024, Finotello et al. 2021, Nururrozi et al. 2024, Stevenson et al. 2021). In particular their spatial distribution, the latter of which for example has proven to predict the response to cytotoxic T-lymphocyte associated protein (CTLA) immune checkpoint inhibitors in human melanomas (Tumeh et al. 2014).

1.4 Canine cutaneous histiocytoma

Canine cutaneous histiocytoma (CCH) is a skin tumour of histiocytic cells (Glick et al. 1976, Kelly 1970, Taylor et al. 1969) of the Langerhans lineage (histiocytoma cells) (Moore et al. 1996). Unique clinical features of this tumour are its common spontaneous regression (Cockerell and Slauson 1979, Kelly 1970, Taylor et al. 1969).

The regression of CCH is thought to be driven by a host-mediated anti-tumour immune response, a theory also supported histologically by the large numbers of lymphocytes observed within regressing tumours (Cockerell and Slauson 1979). These lymphocytes tend to predominantly exhibit a cytotoxic (CD8+) immunophenotype (Moore et al. 1996) which may induce apoptotic cell death of neoplastic cells (Martin De Las Mulas et al. 1998). Investigation of cell death mechanisms in CCH have mainly focused on apoptosis using the TUNEL assay (Guvenc et al. 2002, Pires et al. 2013b) or IHC for Active Caspase 3 (Diehl and Hansmann 2024), with contradictory results between these two methods. The TUNEL assay studies did not show a relationship between apoptosis and regression whereas investigations conducted with Active Caspase 3 IHC identified an increase in apoptosis with regression (Diehl and Hansmann 2024, Guvenc et al. 2002, Pires et al. 2013a). Additionally, the distinct inciting mechanism leading to an immune response directed against histiocytoma cells remains elusive. The most widely accepted mechanism is thought to represent maturation of a subset of neoplastic histiocytoma cells which subsequently activate T cells by presenting neoplastic antigens (Belluco et al. 2020, Kaim et al. 2006, Moore et al. 1996, Pazdzior-Czapula et al. 2014, Pires et al. 2009, Pires et al. 2013b). Other reported mechanisms thought to influence regression, yet would not be able to explain the intense lymphocytic infiltrate, are an imbalance between cell proliferation and apoptotic cell death (Pires et al. 2013a), or compromised angiogenesis (Costa et al. 2020).

1.5 Aims of this study

Investigation of the TME is scarce in canine cutaneous and subcutaneous STSs and in CCH has not yet allowed to fully elucidate the mechanisms leading to regression. This research project is thus composed of two different parts, firstly to investigate the immune infiltrate and subsets of immune cells, including their particular location, in canine cutaneous and subcutaneous STSs, and secondly more closely investigate the causes and/or consequences of the immune infiltrates in CCH.

Our main hypothesis in the STS study was that higher lymphocyte, in particular granzyme B-positive cells (NK and cytotoxic T cells), and lower M2 macrophage infiltrates represent favourable prognostic factors and would be observed in dogs

with a better clinical outcome and also a lower tumour grade. Conversely, we hypothesized that higher numbers of M2 macrophages and Tregs, both considered of anti-inflammatory nature, would be observed in dogs with a worse clinical outcome and a higher grade. Finally, we also wanted to investigate whether these hypotheses held true both for the infiltrating edge of the mass and central tumour regions.

In the CCH study we hypothesized immunogenic cell death, opposed to apoptosis, would, represent the leading cause of the loss of neoplastic histiocytoma cells and promotion of CCH regression via the release of DAMPs, such as HMGB1. In addition, we expected the number of intralesional macrophages to increase progressively with regression due to inflammatory and immune stimulation.

Furthermore, investigations in both these studies were based on the development of a reproducible and reliable methodology to analyse whole slide scanned images with the aid of QuPath, a machine learning program (Bankhead et al. 2017). QuPath is one of the most widely used image analysis software and, in 2021, had already been used in 100 and 53 peer-reviewed publications in the fields of oncology and pathology, respectively. This program enables analysis of files containing billions of pixels and allows reproducible results compared to manual assessment of slides (Humphries et al. 2021).

2 Material and Methods

This study was approved by the School of Biodiversity, One Health & Veterinary Medicine ethics committee (Study Number EA60/23).

2.1 Selection of cases and tissues

The cases included in this study were selected from archived FFPE tissues representing biopsy submissions to the Veterinary Diagnostic Services (VDS), School of Biodiversity, One Health & Veterinary Medicine, University of Glasgow.

2.1.1 Canine cutaneous and subcutaneous soft tissue sarcomas

The VDS database was searched for canine cases containing the keywords “soft tissue sarcoma” or “spindle cell tumour” in their report. Only Small Animal Hospital (SAH) submissions were selected, selection progressed from most recent to earlier submissions and was limited to cutaneous and subcutaneous locations. Reports were reviewed, and grade I and grade III cutaneous and subcutaneous STSs were identified based on the initial diagnosis. Myxosarcomas and liposarcomas were categorically excluded from this study since, in general, such masses commonly exhibit a lower mitotic rate compared to other STS subtypes which can hinder regular grading.

Final selection of the cases was based on (re)examination of all the Haematoxylin and Eosin (H&E) glass slides for each case by two independent observers (SK and AR), and consensual confirmation of the diagnosis and grade (Table 2.1) according to the published grading system in dogs (Dennis et al. 2011, Trojani et al. 1984). The section which had the smallest area of necrosis and the highest number of infiltrating lymphocytes was selected for IHC and image analysis.

It was retrospectively attempted to classify the STS subtypes according to criteria published by Dennis et al.. Tumours were classified as fibrosarcoma, perivascular wall tumours (PWT), peripheral nerve sheath tumours (PNST), pleomorphic sarcoma, undifferentiated sarcomas or mesenchymoma (Dennis et al. 2011). When whorls were detected both around vessels and collagen/nerve

bundles, and in the absence of other distinguishing features, the tumour was classified as “PWT or PNST” (Table 2.2).

Table 2.1 Grading System for Cutaneous and Subcutaneous Soft Tissue Sarcoma in the Dog. From Dennis et al. (2011) and Trojani et al. (1984).

Differentiation score	
1	Sarcomas most closely resembling normal adult mesenchymal tissue
2	Sarcomas for which histologic type can be determined, although differentiation is poor
3	Undifferentiated sarcoma, of unknown type
Mitotic score	**Mitoses per 10 high-power fields (400x; equivalent to 2.37 mm^2 area)**
1	0-9
2	10-19
3	>19
Tumour necrosis score	
0	No necrosis
1	≤50% necrosis
2	>50% necrosis
Histologic grade	**Total score (combined differentiation, mitotic and necrosis scores)**
I	≤3
II	4-5
III	≥6

Table 2.2 Histological features of Cutaneous and Subcutaneous Soft Tissue Sarcoma in the Dog. Adapted from Dennis et al. (2011).

STS subtype	Histological features
Fibrosarcoma	Interwoven bundles, herring-bone pattern, pronounced collagenous stroma
PWT	Staghorn patten, placentoid pattern, perivascular whorls and bundles
PNST	Interwoven bundles, whorls around collagen bundles, Antoni A and B patterns
Pleomorphic sarcoma	Mixture of fibroblastic cells and karyomegalic, cytomegalic, or multinucleate histiocytoid cells in storiform patterns, with variable inflammatory infiltrate
Undifferentiated	No distinct pattern, unknown type
Mesenchymoma	Multiple soft tissue mesenchymal cell types and matrix components including osteoid, chondroid, collagen.

2.1.2 Canine cutaneous histiocytomas

The VDS database was searched for canine cases containing the keyword “histiocytoma”. Selection again progressed from most recent to earlier reports. Reports were reviewed, and both non-regressing and regressing canine cutaneous histiocytomas were identified based on the initial diagnosis and description. Final selection of cases was based on (re)examination of all the H&E

glass slides for each case by two independent observers (SK and AR) and consensual confirmation of the diagnosis. As a next step, all selected cases were assigned a regression group (Table 2.3) according to previously published criteria (Cockerell and Slauson 1979). The section which had the largest surface area and the least amount of crush artefact was selected for IHC and image analysis.

Table 2.3 Histological Grouping System in Canine Cutaneous Histiocytoma. Adapted from Cockerell and Slauson (1979).

Tumour group	Relative number of lymphocytes and macrophages	Pattern of lymphocytes and macrophages infiltrate
I	Minimal to absent	Diffuse and limited to periphery at junction with normal dermis
II	Moderate	Nodular at periphery with mild diffuse component extending towards the centre of the tumour
III	Marked	Nodular both in peripheral and central tumour location
IV	Marked; lymphocytic population greater than histiocytoma cells population	Nodular and extending from the deep margins to the epithelial surface

2.2 Clinical and outcome data for STSs

For each of the STS cases, the SAH database was searched for the exact location of the tumour, absence or presence of evidence of lymph node metastasis at the time of surgery, metastasis in other organs at the time of surgery, recurrence of the tumour, evidence of local lymph node or metastasis to other sites, after the surgery, and if the dog had died, whether the tumour was the cause or not.

In the event of the SAH database lacking complete outcome data, a short questionnaire (Figure 2.1) was sent to the referring veterinary practices to gather information about the status of the dog, including if the dog had been euthanised, if euthanasia was related to the tumour and whether there was local recurrence or distant metastasis, had been observed.

University of Glasgow

School of Biodiversity, One Health & Veterinary Medicine

Tumour-associated inflammation in canine soft tissue sarcomas

(Study number EA60/23)

QUESTIONNAIRE for referring veterinary surgeons

Background and aims: Investigations conducted in humans have indicated that extent and nature of immune infiltrates closely associated with certain tumours, such as breast, colon and ovarian cancer and cutaneous melanoma, may represent biomarkers for survival/prognosis and, in the form of immunotherapy, be exploited in cancer care.

To date, the inflammatory infiltrate in canine soft tissue sarcomas has only been scarcely investigated and correlating the extent of lymphocyte and macrophage subtypes with patient outcome may help improve the future assessment of tumour biopsies in regard to prognosis, risk of recurrence and further implementation of novel immunotherapies.

Aim: This retrospective study examines the inflammatory infiltrate in canine soft tissue sarcomas, in dogs diagnosed with this condition in our institution, and aims to correlate type and extent of infiltrate with tumour outcome.

Questionnaire:

Status of the animal (Dead OR Alive)	
IF animal is dead: date of death	
IF animal is dead: cause of death (Natural OR Euthanasia)	
IF euthanasia: related to tumour (Yes OR No)	
IF euthanasia: presence of local recurrence of tumour (Yes OR No)	
IF euthanasia: presence of distant metastasis (Yes OR No)	

Thank you very much for taking your time to fill in this short questionnaire.

For **further information** please do not hesitate to contact
Katie McNaught (BVMS, MVM, DipECVIM-CA (oncology), MRCVS); Clinician in Small Animal Oncology; Katie.McNaught@glasgow.ac.uk
Samuel Kalpers (DVM, MRCVS); resident in Anatomic Veterinary Pathology; s.kalpers.1@research.gla.ac.uk
Angie Rupp (DVM, Dr med vet, PhD, FRCPath, DipECVP, MRCVS); senior University Clinician in Anatomic Veterinary Pathology; Angelikafrances.Rupp@glasgow.ac.uk

Figure 2.1: Questionnaire for referring Veterinary Surgeons

2.3 Immunohistochemistry

For examining lymphocyte populations, we opted to use CD3 as a T cell marker, CD20 as a B cell marker, FOXP3 as a Treg marker and granzyme B as a combined CTL and NK cell marker. For the macrophage/histiocytic population, we opted to use anti-Iba1 antibody to label all cells from the monocytic/histiocytic lineage (including histiocytoma cells), anti-CD204 antibody to label the general macrophage population, and CD206 as a M2 marker. As the CD3, CD20, CD204 and Iba1 are used routinely in our lab for diagnostic and research purposes, it was not required to optimize the staining protocol for these antibodies. For

Active Caspase 3, FOXP3, HMGB1 and granzyme B, an optimization step was carried out by SK, AR and the VDS histology laboratory staff to allow correct identification of the targeted cells and reduce any background staining on appropriate control tissues (Table 2.4). The optimization process was achieved by using various primary antibody concentrations and antigen retrieval protocols. The protocol that allowed to stain the targeted cells best with the lower background staining in the positive control material was then applied on the sections used in the STS and CCH studies (Table 2.4).

For immunohistochemistry (IHC – performed by the VDS histology laboratory staff), sections were cut at a 4µm thickness and mounted on charged slides. Antigen retrieval was performed using heat-induced epitope retrieval. Depending on the antibody (Table 2.4), sections were treated at full pressure for 90 seconds at 125°C in the Access Retrieval Unit (Menarini, Florence, Italy) with Sodium Citrate buffer (pH 6) or EDTA (pH9). The sections were then rinsed in TRIS Tween buffer (pH 7.5, manufactured in house). The following steps were automated by a machine (AutostainerLink 48, Agilent Dako Pathology Solutions, Santa-Clara, California, USA). The sections were treated for 5 minutes at room temperature with 3% hydrogen peroxide in phosphate buffered saline (PBS) to quench endogenous peroxidase activity. After washing twice with TRIS Tween buffer (pH 7.5), sections were then incubated for 30 minutes at room temperature with the primary antibody (Table 2.4) diluted in Dako REAL Antibody Diluent (ref. S2022, Agilent Dako Pathology Solutions, Santa-Clara, California, USA) then washed again with TRIS Tween buffer (pH 7.5).

For the anti-FOXP3 antibody only, the primary antibody was in first instance detected with 1:100 biotinylated rabbit anti-rat IgG antibody (H+L) (Vector Laboratories, Newark, California, USA) diluted in PBS for 30 minutes, then washed with TRIS Tween buffer (pH 7.5). Next, for all other primary antibody detection (including detection of the biotinylated rabbit anti-rat IgG antibody applied for FOXP3), sections were incubated with EnVision+ System HRP labelled polymer anti-rabbit or anti-mouse (Table 2.4) secondary antibody (Agilent Dako Pathology Solutions, Santa-Clara, California, USA) for 30 minutes at room temperature, then washed with TRIS Tween buffer, followed by two 5 minute incubations with 3,3'-diaminobenzidine (DAB) substrate-chromogen (EnVision+ System, Agilent Dako Pathology Solutions, Santa-Clara, California, USA). Finally,

sections were rinsed twice with distilled water for 5 minutes, counterstained using Gill's haematoxylin, and automatically cover-slipped using ClearVue cover slipper (Epredia, Runcorn, UK).

The IHC staining runs were performed independently for each marker and subproject (STS versus CCH project) in batches of 30 cases each, accompanied by adequate positive control material (Table 2.4) and one negative control per section, the latter of which followed the same protocol with antigen retrieval carried out with pH6 citrate buffer, and replacement of the primary antibody by Dako REAL Antibody Diluent (ref. S2022, Agilent Dako Pathology Solutions, Santa-Clara, California, USA).

For every stain, individual slides were checked for adequate staining, presence of unexpected background stain and appropriate location of staining in the cells.

Table 2.4 Primary Antibodies Used for Immunohistochemistry.

Antigen	Clone	Catalogue number	Supplier	Secondary antibody	Dilution	Antigen retrieval	Positive control material (canine tissues)	Project
CD3	Polyclonal	A0452	Dako	Rabbit	1:100	Sodium Citrate buffer pH6	Lymph node and tonsil	STS and CCH
CD20	Polyclonal	PA5-16701	Fisher	Rabbit	1:600	Sodium Citrate buffer pH6	Lymph node and tonsil	STS
FOXP3	Monoclonal	FJK-16s	Invitrogen	Rat	1:800	EDTA pH9	Lymph node and histiocytoma	STS
Granzyme B	Polyclonal	ab4059	Abcam	Rabbit	1:400	EDTA pH9	Reactive and normal lymph nodes	STS
Iba1	Polyclonal	019-19741	Wako (Alpha Laboratories)	Rabbit	1:600	Sodium Citrate buffer pH6	Lymph node	CCH
CD204	Monoclonal	SRA-E5	Transgenic KT022	Mouse	1:800	EDTA pH9	Lymph node and tonsil	STS and CCH
CD206	Polyclonal	ab64693	Abcam	Rabbit	1:1200	Sodium Citrate buffer pH6	Lung and granulation/early scar tissue	STS
Active Caspase 3	Polyclonal	AF835	R&D	Rabbit	1:250	Sodium Citrate buffer pH6	Thymus and lymphoma	CCH
HMGB1	Monoclonal	ab79823	Abcam	Rabbit	1:800	Sodium Citrate buffer pH6	Spleen and liver infected with CAV2	CCH

CAV2: Canine Adenovirus 2; CCH: Canine cutaneous histiocytoma; STS: soft tissue sarcoma.

2.4 Blinding and scanning of slides

To ensure blinded analysis, each case was attributed a random number prior to scanning (by AR), and all scanned slides, comprising the complete set of markers for each case, were labelled by this number.

All slides were scanned by the VDS histology laboratory staff at x40 magnification on Motic Easyscan Infinity 60 (Motic Europe, Barcelona, Spain), which generated image files in .svs format. All the scanned slides were checked individually by SK for appropriate image quality. Image quality was considered adequate if the scan allowed correct identification of the cells and location of the staining within the cells (membranous, cytoplasmic or nuclear). Appropriate focus over the tumour area was also evaluated and if the scan was out of focus or of poor quality, the scanning process was repeated until satisfactory results were achieved.

2.5 Image analysis

QuPath (version 5.1) (Bankhead et al. 2017), one of the most widely used image analysis software programmes for whole slide images (Humphries et al. 2021), was used for the analysis of the IHC marker on scanned slides. As many publications have validated QuPath on immunolabelled sections with a variety of IHC markers, either with the cell detection (Avallone et al. 2024, Humphries et al. 2021, Li et al. 2026, Liu et al. 2020, Roberti et al. 2020) or the pixel classifier tools (Ducor et al. 2026, Kang et al. 2025, Mondal et al. 2023), an internal validation protocol was not considered necessary.

Image analysis of CCHs and STSs was performed in separate QuPath projects, with different QuPath projects also used for each IHC marker and images opened and analysed in the Brightfield (H-DAB) image type.

The outcome of the training was considered satisfactory when approximately, and subjectively, more than 95 % of the targeted areas on all sections of the same IHC marker were identified by the object or pixel classifier. The training was performed by SK alone. When they are generated, the classifiers and cell detection tools give the same result each time they are applied with identical

parameters. Hence, when the training was considered satisfactory, the pixel/object classifier generated or the cells detection parameters (more details about the methodology bellow) was applied once.

2.5.1 Canine cutaneous and subcutaneous soft tissue sarcomas

Analysis of the whole section scanned images was performed with the aim of following the guidelines published by the International Immuno-Oncology Biomarkers Working Group (Hendry et al. 2017b). Since it is impossible to distinguish tumoral stroma and neoplastic cell areas in STSs, these areas were not differentiated in our image analysis (Figure 2.2).

1. Immune cells (ICs) are evaluated separately within the borders of the invasive margin (if present in the section examined) and within the central tumour (represents the remaining neoplastic tissue).
2. The invasive margin (IM) corresponds to a 1mm region centred on the border separating the malignant cell nests from the normal host tissue. The central tumour (CT) represents the remaining tumour tissue.
3. Exclude ICs peripheral to the tumour border (representing tissue over 0.5 mm from the margin, except immediately adjacent to the border).
4. Exclude ICs in zones with crush artifacts, necrosis and hyalinization.
5. Assessment of one section (4-5 μm thick, at magnification 200-400x) is considered sufficient. Although assessing more sections would be preferable.
6. Do not focus on hotspots, use the entire tumour section.

Figure 2.2 Guidelines for the assessment of whole section scanned images modified and adapted from the International Immuno-Oncology Biomarkers Working Group (Hendry et al., 2017)

After loading all the images for a single IHC marker into a QuPath project, the tumour margin was drawn manually and overlined by the brush tool at magnification 0.5x to create the 1 mm thick invasive margin (IM) annotation on the section of choice. Subsequently, an inverse annotation was generated to create the central tumour (CT) annotation (Figure 2.3.A).

Next, a pixel classifier was trained with the purpose of differentiating optically empty areas on the section from areas containing neoplastic and normal tissue. The pixel classifier initially was trained on one randomly selected section where one area was labelled as “tissue”, and another area was labelled as “empty” (Figure 2.3.B). The pixel classifier subsequently was applied to all sections to create annotations with a minimum object size of 10000 μm^2 and minimum hole

size of 10000 μm^2 (Figure 2.3.C), after which the "empty" annotations and previous CT and IM annotations were deleted and only areas identified as "tissue" both in the CT and IM were kept.

The next step consisted of the removal of necrosis, crush artefacts and areas of hyalinization. Tiles were generated in CT and IM areas of all slides by using the "SLIC superpixel" tool with the following parameters: Gaussian sigma = 5 µm, Superpixel spacing = 200 µm, Number of iterations = 10, Regularization = 0.25. Intensity features were then generated with the following resolution: preferred pixel size = 2µm, Region = ROI, Tile diameter = 25 µm; followed by channels/colour transformations: Optical density sum, Haematoxylin (colour deconvolved), Eosin (colour deconvolved), Residual (colour deconvolved), red, green, blue, hue (mean only), saturation, brightness; and with the following (basic) read-out features: mean, standard deviation, min & max, median (Table 2.5). For each IHC marker, an object classifier, using the tiles previously generated, was then created and trained on all the sections of the same IHC marker, which were in turn annotated with areas of "tumour" and "necrosis/artefact/hyalinisation" with the aim of having equal training data for regions of "tumour" tissue and regions of "necrosis/artefact/hyalinisation". The object classifier then was trained until satisfactory differentiation could be achieved on all the sections (Figure 2.3.D). Annotations ("tumour" vs "necrosis/artefact/hyalinisation") were then created based on the detections of the object classifier, and all the annotations were removed except the ones generated for "tumour" tissue in the CT and IM.

The final step of image analysis in the STS cohort consisted of the detection of positive cells. For each IHC marker, a pixel classifier (2.09 µm/pixel) was trained on selected sections, containing representative positive and negative immunolabelling, with the aim of having equal training areas between the "positive" and "negative" areas on sections stained for CD3 (n=2), CD20 (n=2), CD204 (n=3), CD206 (n=3), FOXP3 (n=4) and granzyme B (n=3). Since the IHC marker for granzyme B, and only for granzyme B, showed a particular focal to multifocal, granular, cytoplasmic pattern, and additional mild non-specific labelling of the red blood cells was observed, the pixel classifier was trained differently for this IHC marker with "positive", "negative" and "red blood cell" areas, also aiming to have equal training areas between the "positive" and

“negative” regions and foci containing “red blood” cells. The pixel classifier subsequently was applied to all the sections and trained until a satisfactory differentiation could be achieved on all the sections (Figure 2.3.E). Annotations were created based on the detections by the pixel classifier with a minimum object size of 30 μm^2 and minimum hole size of 30 μm^2 for all IHC markers. The last step consisted of removal of all annotations except the CT and IM tumour areas and respective “positive cell” areas generated for the CT and IM.

For each IHC marker, the image, classification, parent and area (μm^2) measurements obtained in viable and assessable tumour regions was exported from QuPath in a .tsv file format.

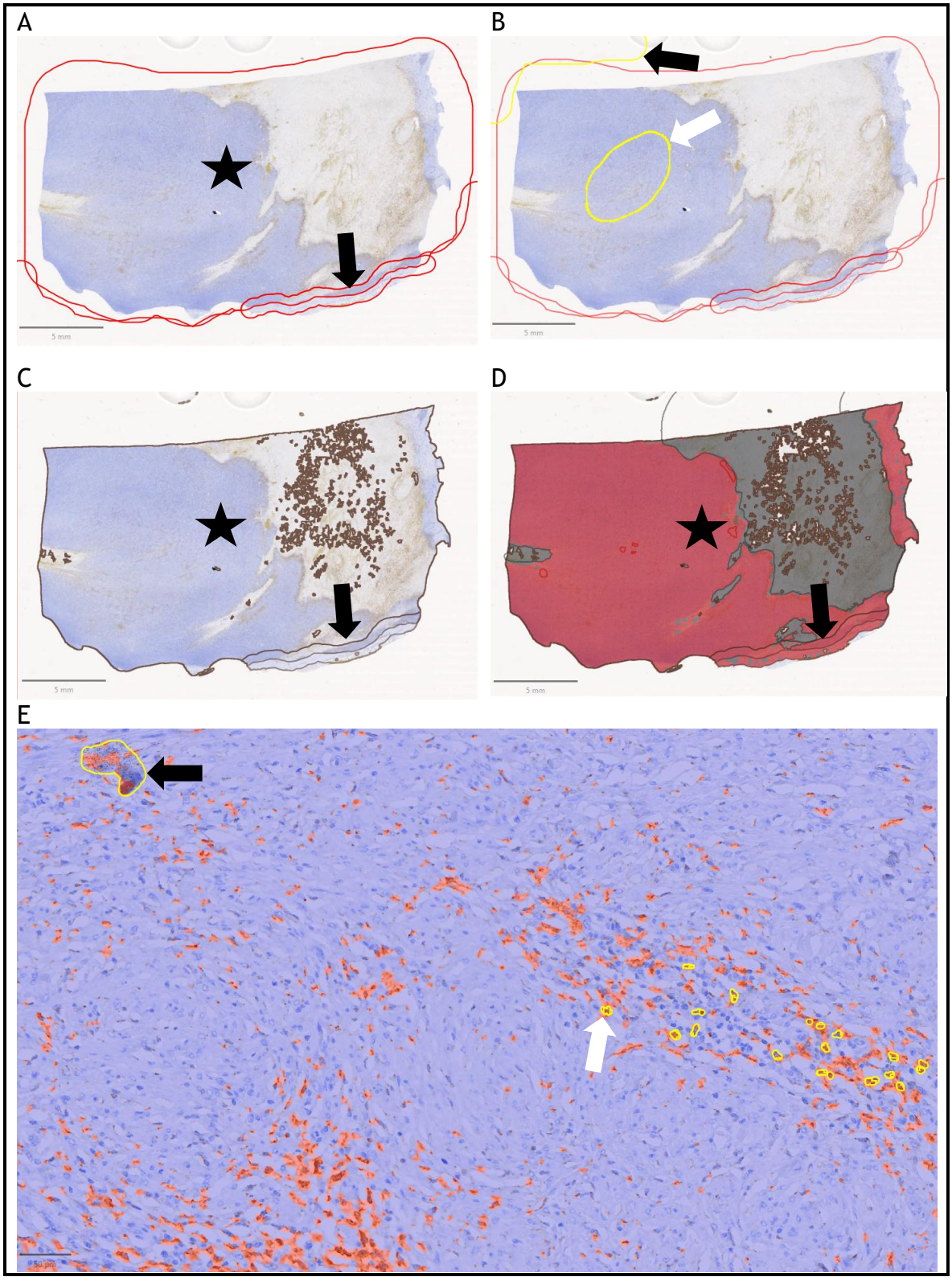

Figure 2.3 QuPath training steps for canine cutaneous and subcutaneous soft tissue sarcomas.

A. Selection of tumour with invasive margin (black arrow) and central tumour (black star). CD204, STS29. Bar = 5 mm.
B. Annotations (yellow lines) used to train the tissue detection pixel classifier, with "tissue" areas (white arrow) and "empty" areas (black arrow). CD204, STS29. Bar = 5 mm.
C. Annotation (brown lines) after applying tissue detection pixel classifier, with invasive margin (arrow) and central tumour (star). CD204, STS29. Bar = 5 mm.
D. Detection of necrosis (grey areas) and tumour (red areas) with the object classifier. CD204, STS29. Bar = 5 mm.

E. Training of positive areas by pixel classifier. Red = detection of positive areas. Blue = detection of negative areas. Yellow lines depict positive (white arrow) and negative (black arrow) training annotations. CD204, STS26. Bar = 50 µm.

2.5.2 Canine cutaneous histiocytomas

After loading all images for a single IHC marker into a QuPath project, the section of choice for each case was selected manually with the brush tool (Figure 2.4.A).

The first step consisted of training QuPath to differentiate "tissue" from the "empty" areas. Tiles were generated for all the sections of the same IHC marker by using the "SLIC Superpixel" tool with the same parameters as used in the STSs (Table 2.5). In short, an object classifier was created and trained on one randomly selected section which was annotated with "tissue" and "empty" areas. The object classifier was then applied to the remaining sections (Figure 2.4.B) and annotations were created based on the detection by the object classifier. Finally, all annotations were removed except the ones identifying the "tissue".

The second step consisted of training QuPath to differentiate tumour tissue from regular cutaneous and subcutaneous areas. Again, tiles were generated on the tissue sections by using the "SLIC superpixel" and with the same parameters as step 1 (Table 2.5), yet this time the object classifier created was trained on all the sections of the same IHC marker which had their "tumour" and "non-tumour" regions annotated with the aim of having equal training areas for these two criteria. The object classifier then was trained until a satisfactory differentiation could be achieved on all the sections of the same IHC marker (Figure 2.4.C), was applied to the sections, annotations for "tumour" and "non-tumour" tissue created, and all the annotated regions removed except those generated for the "tumour" areas.

Necrosis causes loss of integrity of the cells, and impaired staining and assessment of the cellular compartments investigated (nucleus, cytoplasm, membranous) due to effacement of these structures. Thus, the third step consisted of training QuPath to differentiate viable and regular tumour tissue from necrotic, inflammatory (presence of neutrophils), out of focus, and crushed areas. For this, tiles were generated on the tissue sections by using the "SLIC

superpixel" tool with slightly different parameters (Table 2.5). An object classifier was created and trained on sections, containing representative positive and negative immunolabelling, with IHC markers against Active Caspase 3 (n=12), CD3 (n=12), CD204 (n=12) and HMGB1 (n=10). The sections were annotated with "tumour" and "necrotic/inflammatory/out of focus/crushed" areas with the aim of having equal training areas between the two areas and were trained until a satisfactory differentiation could be achieved on all the sections of the same IHC marker (Figure 2.4.D). The object classifier generated was then applied to the sections of the same marker (Figure 2.4.E), annotations were created based on the detection of the object classifier, and again all annotations removed except the ones generated for the "tumour" areas.

The fourth step consisted of training QuPath to differentiate the tumour areas from areas containing fibrosis. For this, tiles were generated on the sections by using the "SLIC superpixel" tool yet again with a slight modification of parameters (Table 2.5) and an object classifier was created and trained on sections, containing representative positive and negative immunolabelling, with IHC markers against Active Caspase 3 (n=10), CD3 (n=16), CD204 (n=6) and HMGB1 (n=13). The sections were annotated with "tumour" and "collagenous" areas with the aim to have comparable training data for both these parameters. The object classifier was trained until a satisfactory differentiation could be achieved and then applied to the sections of the same marker. Annotations then were created based on the detections of the object classifier, and all the annotations removed except those generated for the "tumour" areas.

To select mostly the tumour and remove the hair follicles and epidermis which had been detected by the previous object classifier, the fifth step in assessing the histiocytomas consisted of splitting ("split" tool) the remaining "tumour" annotations into smaller, non-contiguous, individualized annotations and select the "main area" of the tumour by deleting all the annotations except the "main area". If the "main tumour" was split in two or even more annotations, the annotations were kept and merged into one (Figure 2.4.F).

The sixth and final step of image analysis consisted of the detection of positive cells, which, similar to the STSs was achieved by training a pixel classifier (1.04 µm/pixel). For all IHC markers except HMGB1 (see below), three sections per

IHC marker were selected with the aim of having equal training areas between the “positive” and “negative” areas. The pixel classifier generated was applied to the sections and trained until a satisfactory differentiation could be achieved on all the sections of the same IHC marker. Next, annotations were created on all sections of the same IHC marker based on the detection of the pixel classifier with a minimum object size of 5, 5 and 30 μm^2 and minimum hole size of 5, 5 and 30 μm^2 for Active Caspase 3, CD3 and CD204, respectively. Then, all remaining annotations were removed except the “tumour” areas and “positive” areas generated by the pixel classifier.

With HMGB1 present both in the nucleus and in the cytoplasm and the distribution pattern of interest, a positive cell detection tool was used to analyse the immunolabeling pattern. The setup parameters were as follows: Detection image = Optical density sum; Requested pixel size = 1 µm; Nucleus parameters: Background radius = 10 µm; median filter radius = 0 µm; sigma = 1.55 µm; minimum area = 10 µm; maximum area = 400 µm; Intensity parameters: Threshold = 0.1; max background intensity = 2; split by shape. General parameters: Smooth boundaries; Make measurements. Intensity threshold parameters: Score compartment = Nucleus: DAB OD mean; Threshold 1+ = 0.1; Threshold 2+=0.4; Threshold 3+=0.6 (Table 2.6).

For each IHC marker, the image metadata and measurements (μm^2) were exported from QuPath into a .tsv file format.

Table 2.5 Tiles SLIC Superpixel Parameters and Intensity Features for Canine Cutaneous and Subcutaneous STS and CCH Image Analysis.

SLIC superpixel parameters for Soft Tissue Sarcoma and First and Second Step of Histiocytoma		
	Gaussian sigma	5 µm
	Superpixel spacing	200 µm
	Number of iterations	10
	Regularization	0.25
SLIC superpixel parameters for the Third Step of Histiocytoma		
	Gaussian sigma	5 µm
	Superpixel spacing	50 µm
	Number of iterations	8
	Regularization	0.25
SLIC superpixel parameters for the Fourth Step of Histiocytoma		
	Gaussian sigma	5 µm
	Superpixel spacing	25 µm
	Number of iterations	10
	Regularization	0.25
Intensity features		
	Resolution	
	Preferred pixel size	2 µm
	Region	ROI
	Tile diameter	25 µm
	Channels/colour transform	
	Optical density sum	
	Haematoxylin (colour deconvolved)	
	Eosin (colour deconvolved)	
	Residual (colour deconvolved)	
	Red	
	Green	
	Blue	
	Hue (mean only)	
	Saturation	
	Brightness	
	Basic features	
	Mean	
	Standard deviation	
	Min & max	
	median	

Table 2.6 HMGB1 Positive Cell Detection Parameters.

Setup parameters		
	Detection image	Optical density sum
	Requested pixel size	1 µm
Nucleus parameters		
	Background radius	10 µm
	Use opening by reconstruction	
	Median filter radius	0 µm
	Sigma	1.55 µm
	Minimum area	10 µm
	Maximum area	400 µm
Intensity parameters		
	Threshold	0.1
	Max background intensity	2
	Split by shape	
Cell parameters		
	Cell expansion	3 µm
	Include cell nucleus	
General parameters		
	Smooth boundaries	
	Make measurements	
Intensity threshold parameters		
	Score compartment	Nucleus: DAB OD mean
	Threshold 1+	0.1
	Threshold 2+	0.4
	Threshold 3+	0.6

DAB: 3,3'-diaminobenzidine. OD: Optical density

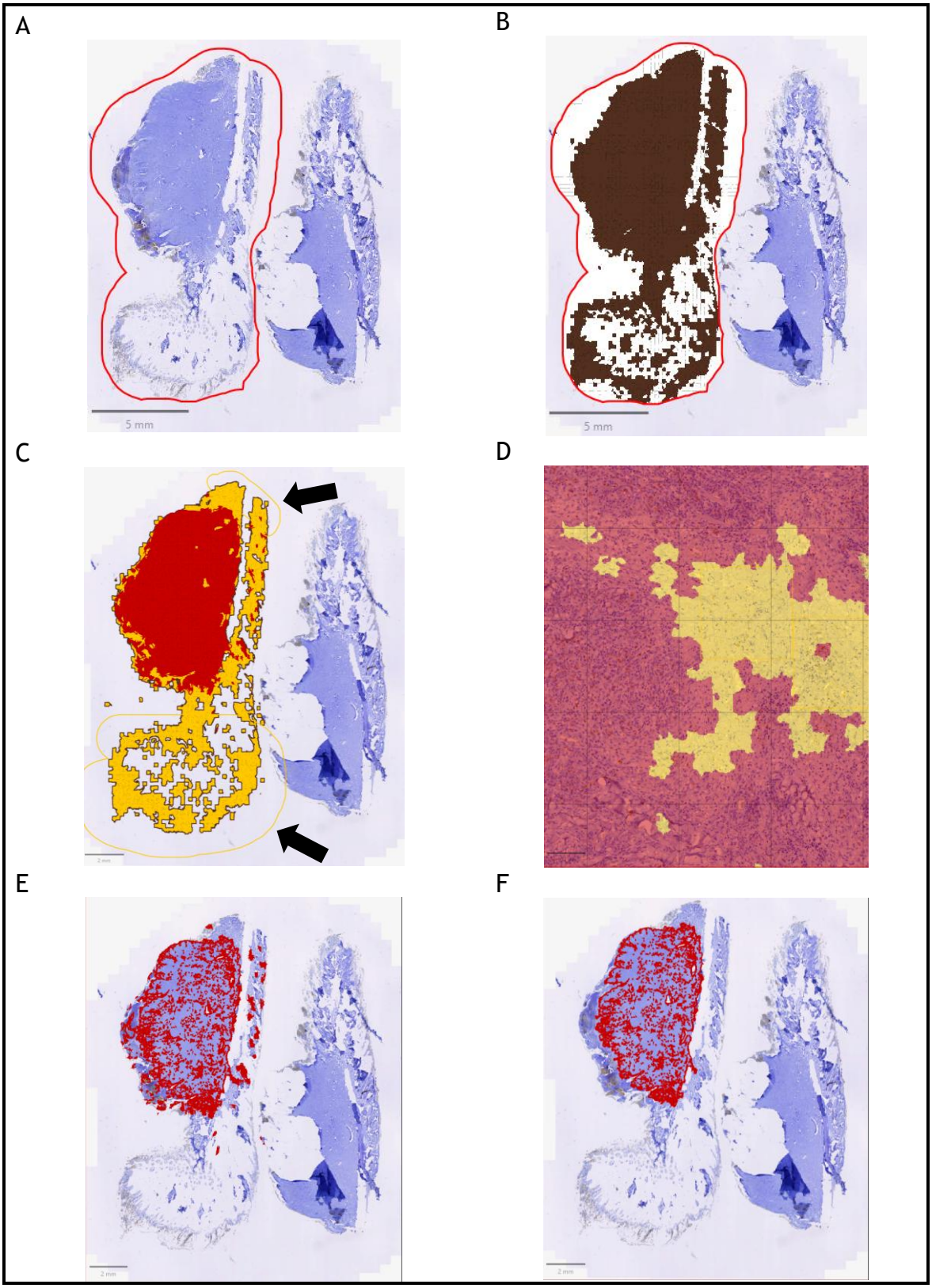

Figure 2.4 QuPath training steps for CCH

A. Manual selection of the section of interest (red outline). CD3, CCH1. Bar = 5 mm.
B. First step of image analysis: the brown areas represent the tiles detected as "tissue" and the white areas represent the tiles detected as "empty" areas in the area of interest (red outline) after application of tissue detection object classifier. CD3, CCH1. Bar = 5 mm.
C. Second step of image analysis: the yellow outlined areas (black arrow) represent "non-tumour" training areas. The yellow areas are the tiles detected as "non-tumour" areas and the red areas are the tiles detected as "tumour" areas by the object classifier. CD3, CCH1. Bar = 2 mm.

D. Third step of image analysis: the yellow areas represent the tiles detected as "necrotic/inflammatory/out of focus/crushed" and the red areas represent the tiles detected as "tumour" by the object classifier. CD3, CCH30. Bar = 100 µm.
E. Fourth step of image analysis: "Tumour" areas (red outline) after removal of the generated "necrotic/inflammatory/out of focus/crushed" areas by the object classifier. CD3, CCH1. Bar = 2 mm.
F. Sixth step of image analysis: Final tumour area is outlined red after splitting of the generated "tumour" area during the fifth step and deletion of all the areas except the main tumour area. CD3, CCH1. Bar = 2 mm.

2.6 Statistical analyses

The data (.tsv file format) were transferred into Excel and saved in a .csv file format.

Statistical analyses was performed using R (version 4.4) (R Core Team 2019) combined with the RStudio interface and Tidyverse R package (Wickham et al. 2019).

For all IHC markers evaluated, each dataset and its logarithmic value underwent a Shapiro-Wilk test for normality. A p-value < 0.95 was considered to be a normal distribution, whereas a result ≥ 0.95 was considered to represent an abnormal distribution.

For all other statistical analysis, results were considered to be significant for a p-value < 0.05, to represent a tendency for a p-value ≥ 0.05 and < 0.10 and to be non-significant for a p-value ≥ 0.10.

2.6.1 Cutaneous and subcutaneous canine soft tissue sarcoma

A Wilcoxon signed-rank test was performed to compare the positive pixel areas (%; positive pixel area/neoplastic area) for IHC markers CD20, CD3, FOXP3, granzyme B, CD204, CD206 and the FOXP3 to CD3 ratio between the CT and IM (combining grade I and grade III tumours), between the CT of grade I and grade III tumours, and between the IM of grade I and grade III tumours.

Given the relatively small study population, partially exacerbated by incomplete data sets (see results) and the current guidelines recommending to use more than 500 cases to evaluate the outcome by performing a logistic regression model (Collins et al. 2016, van Smeden et al. 2019), any data associated with

outcome and more specifically evidence of recurrence after the surgery, distant metastasis after the surgery and whether the tumour was responsible for the euthanasia of the dog, was interrogated only in a descriptive manner and by including the median and interquartile range.

2.6.2 Canine cutaneous histiocytoma

To compare the data obtained between the regression groups, a Kruskal-Wallis rank sum test was performed for CD3, CD20, Active Caspase 3 positive pixel areas (%; positive pixel area/neoplastic area), HMGB1 positive cell areas (%; positive pixel area/cell area), and the median of “DAB OD mean” of cytoplasmic, nuclear and nuclear to cytoplasmic ratios (N/C ratio) for HMGB1-positive pixels. An ANOVA test was performed for the median of “DAB OD mean” of cellular HMGB1. If the Kruskal-Wallis rank sum test or ANOVA analysis were significant, a Dunn test or Post-Hoc test for multiple comparisons was performed, respectively, and the unadjusted p-value assessed in order to interpret the results.

3 Results

3.1 Canine cutaneous and subcutaneous soft tissue sarcomas

3.1.1 Sample population and clinical data

The STS study comprised 30 cases (n=15 grade I and n=15 grade III), for three of which clinical information could not be retrieved due to corruption of the database. Moreover, due to technical issues (tissue fragmentation during the antigen retrieval process), case 7 was replaced by case 31, whose IHC labelling was conducted separately of the remaining 29 cases (which were all stained in the same run). As tissue blocks/sections for analysis were selected based on the section of the case which had the least amount of necrosis and the highest number of lymphocytes, the IM was not present in all, but a substantial proportion of the sections analysed (n=23/30).

The final sample population comprised 7 female (5 neutered and 2 entire) and 23 male (9 neutered and 14 entire) dogs of 18 different breeds. The age ranged from 3 to 14.2 years with a median of 9.7 years and interquartile range (IQR) of 4.5 years (Table 3.1). Seventeen cases had a tumour on a limb, eight on the trunk (four axillary, two inguinal, one thorax, one perianal), three on the head and two on the tail. None of the dogs had evidence of lymph node metastasis by fine needle aspirate or distant metastasis on computed tomography scan at the time of surgery.

Of the dogs with grade I STS, there were 9, 3, and 1 tumours with histological features compatible with PWT, fibrosarcoma and PNST, respectively. For two tumours, it was not possible to differentiate between PWT and PNST with HE staining alone. Of the dogs with grade III STS, there were 3, 1 and 1 tumours with histological features compatible with PWT, PNST and fibrosarcoma, respectively. There were 10 undifferentiated sarcomas, all of which were grade III tumours (Table 3.1).

For the outcome data, the period of follow-up ranged from 1 to 104 months with a median of 13 months. Of the cases with complete records (n=27), outcome data for local tumour recurrence could be obtained in 15 cases (five grade I, ten

grade III). Of these, recurrence was reported in five dogs (33.3%, one grade I, four grade III); outcome data for local lymph node metastasis could be obtained from the SAH database in eight cases (two grade I, six grade III) and was only reported in one dog (12.5%; one grade III, hence not further examined); outcome data for distant metastasis could be obtained in nine cases (two grade I, seven grade III) of which four dogs (44.4%, four grade III) were diagnosed with distant metastases. Fourteen cases (six grade I, eight grade III) with complete records were dead at the time of the study and death was attributed to the tumour in six (42.8%, two grade I, four grade III) of these (Table 3.1).

Table 3.1 Clinical data for STS cases.

Case	Breed	Sex	Age (years)	Location	Classification	Grade	Invasive margin in the block selected	Local recurrence after surgery	Regional lymph node metastasis after surgery	Distant metastasis after surgery	Death caused by tumour
1	Crossbreed	MN	4.1	Right hind leg	Undifferentiated	III	Y	Y	/	Y	Y
2	Border Collie	FN	13.8	Right muzzle	Undifferentiated	III	Y	/	/	/	/
3	Crossbreed	ME	12	Right shoulder	Undifferentiated	III	Y	/	/	/	N
4	Boxer	MN	7.3	Right forelimb	Fibrosarcoma	I	Y	N	/	/	/
5	Crossbreed	ME	12.9	Left tail base	PWT	III	N	N	N	N	N
6	Crossbreed	MN	12	Left thigh	PNST	I	Y	/	/	/	Y
8	Tibetan Terrier	MN	12.4	Right hind limb	PWT	I	Y	/	/	/	/
9	Golden Retriever	MN	7.9	Perianal	Undifferentiated	III	Y	N	N	Y	/
10	Golden Retriever	ME	9.7	Left humerus	Fibrosarcoma	III	Y	N	N	Y	/
11	Whippet	FN	7.4	Left scapula	Undifferentiated	III	Y	N	N	N	N
12	Labradoodle	ME	10	Head, dorsal to the orbit	Undifferentiated	III	Y	/	/	/	/
13	German Shepherd	ME	9.6	Left hindlimb	PNST or PWT	I	Y	/	/	/	/
14	Lhasa Apso	ME	13.2	Left forelimb	PWT	I	N	/	/	/	/
15	Golden Retriever	ME	9.7	Thorax	PWT	III	Y	Y	/	/	/
16	Collie	FE	11.4	Right inguinal	PWT	III	N	Y	/	/	Y
17	Poodle	FN	14.2	Left elbow	PWT	I	Y	/	/	/	/
18	Labrador	FN	3	L medial elbow	Undifferentiated	III	Y	N	N	Y	/
19	Lurcher	ME	7.9	Right forelimb	PWT	I	Y	Y	/	/	N
20	Schnauzer	ME	10.2	Left carpus	PNST	III	Y	/	/	/	N
21	Golden Retriever	ME	7.7	Left thorax	PWT	I	Y	N	N	N	N
22	Boxer	MN	5.9	Tail base	PWT	I	Y	/	/	/	/
23	Crossbreed	MN	13.7	Thorax	Undifferentiated	III	Y	/	/	/	/
24	Rottweiler	ME	11	Right inguinal	Fibrosarcoma	I	N	/	/	/	/
25	Terrier	ME	10.3	Right forelimb	PNST or PWT	I	Y	/	/	/	/

26	Collie	FN	7.1	Left flank	Fibrosarcoma	I	Y	N	/	/	N
27	Retriever	ME	7	Right elbow	PWT	I	Y	N	N	N	N
28	Yorkshire Terrier	ME	3.6	Top of the head	Undifferentiated	III	N	Y	/	/	Y
29	Pug	FE	8	Left axillary	Undifferentiated	III	N	N	Y	N	Y
30	Lurcher	MN	12.3	Right elbow	PWT	I	N	/	/	/	/
31	Collie	MN	9.2	Right carpus	PWT	I	Y	/	/	/	Y

FE: Female Entire. FN: Female Neutered. ME: Male Entire. MN: Male Neutered. /: missing data. Y: Yes. N: No. PWT: Perivascular wall tumour. PNST: Peripheral nerve sheath tumour.

3.1.2 Analysis of lymphocyte and macrophage subsets in comparison to the tumour region, grade and outcome

The outcome of the immunohistochemical staining revealed moderate to strong membranous staining and weak cytoplasmic staining for CD3, CD20, CD204, CD206; moderate to strong, cytoplasmic staining for granzyme B, forming multifocal cytoplasmic globules; moderate to strong nuclear staining for FOXP3. For CD206 and granzyme B staining, there is a moderate and diffuse non-specific background staining throughout the sections and for granzyme B staining, there is a moderate non-specific background staining in the erythrocytes located in the blood vessels (Figure 3.1).

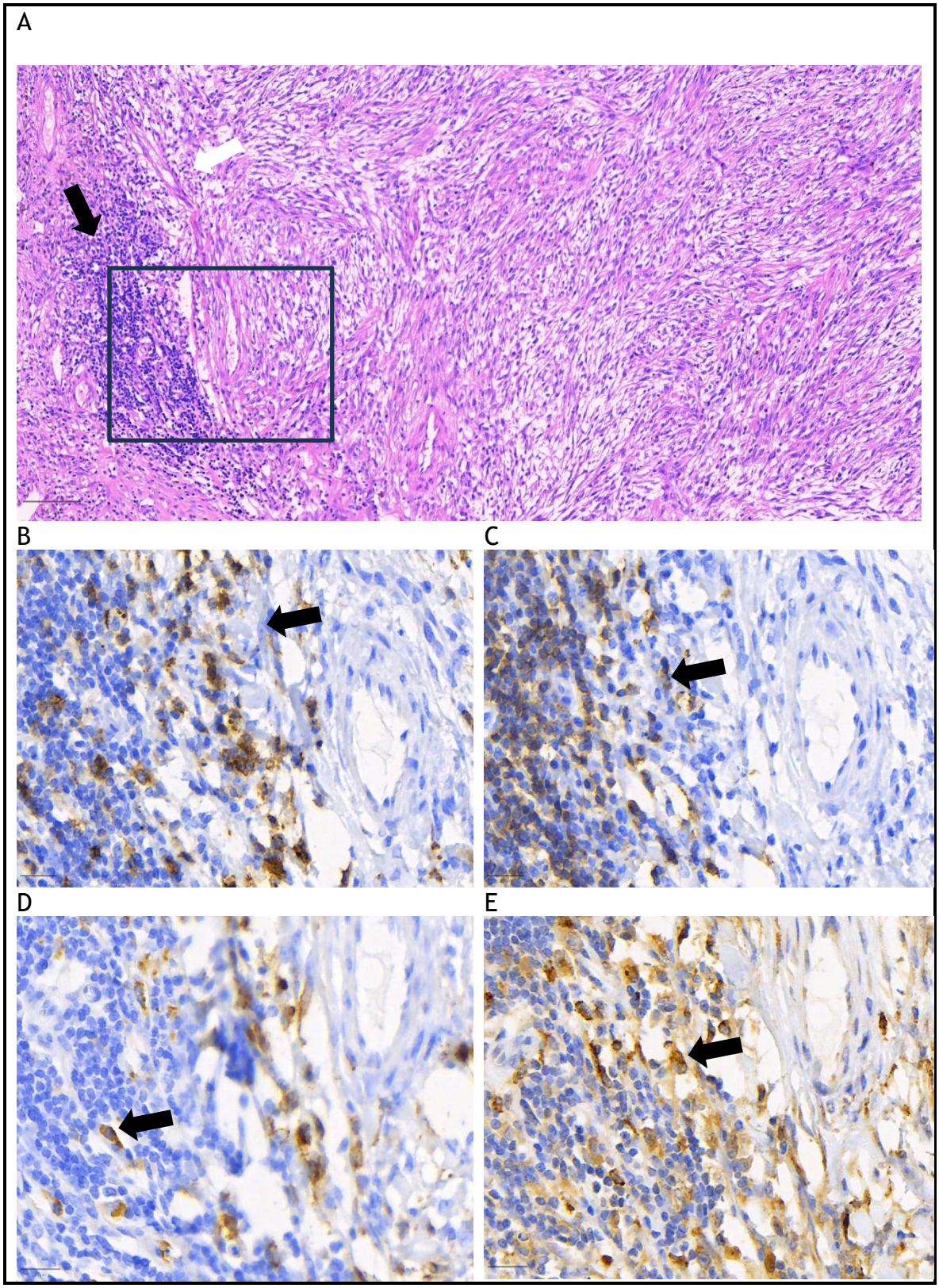
A
B
C
D
E

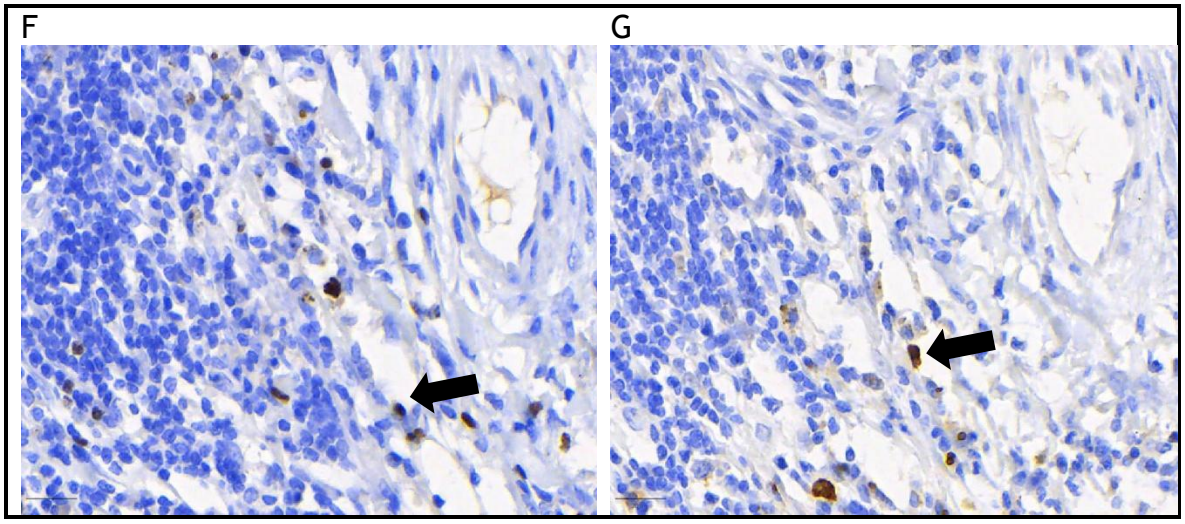

Figure 3.1 Example of histology and IHC of cutaneous and subcutaneous STS

A. Undifferentiated grade III STS with an infiltrate of immune cells forming a nodular aggregate (black arrow). The rectangle represents the fields in B-G. STS2, HE. Bar = 100 µm
B. Lymphocytes exhibit strong membranous and moderate cytoplasmic staining (black arrow). STS2, CD3. Bar = 20 µm
C. Lymphocytes exhibit strong membranous and moderate cytoplasmic staining (black arrow). STS2, CD20. Bar = 20 µm
D. Macrophages exhibit strong membranous and moderate cytoplasmic staining (black arrow). STS2, CD204. Bar = 20 µm
E. Macrophages exhibit strong membranous and moderate cytoplasmic staining (black arrow). STS2, CD206. Bar = 20 µm
F. Lymphocytes exhibit strong nuclear staining. STS2, FOXP3. Bar = 20 µm
G. Lymphocytes exhibits strong cytoplasmic and coarsely granular staining (black arrow). STS2, granzyme B. Bar = 20 µm

3.1.2.1 Overview of cellular infiltrates in all regions and regardless of tumour grade

When assessing all tumours (regardless of grade), the general T cell and B cell markers, CD3 and CD20, respectively, as well as markers for the specific T-cell populations Tregs and joint CTL and NK cells, FOXP3 and granzyme B, respectively, exhibited a statistically significantly higher positive pixel percentage in the IM compared to the CT area (Table 3.2 andFigure 3.2). In contrast to this, both the general and the M2 macrophage markers, CD204 and CD206, had a higher positive pixel percentage in the CT areas when compared to the IM, but this was not statistically significant (Table 3.2 andFigure 3.2). The ratio of FOXP3 to CD3 positive pixel percentage was not significantly different between the tumour areas, however there was a trend of a higher percentage of T-regs in the IM when compared to the CT region (Table 3.2).

The interquartile range (IQR) was higher in IM than in CT areas for CD3, CD20, FOXP3, granzyme B and the ratio between FOXP3 and CD3, whereas it was higher in CT than in IM areas for CD204 and CD206 (Table 3.2).

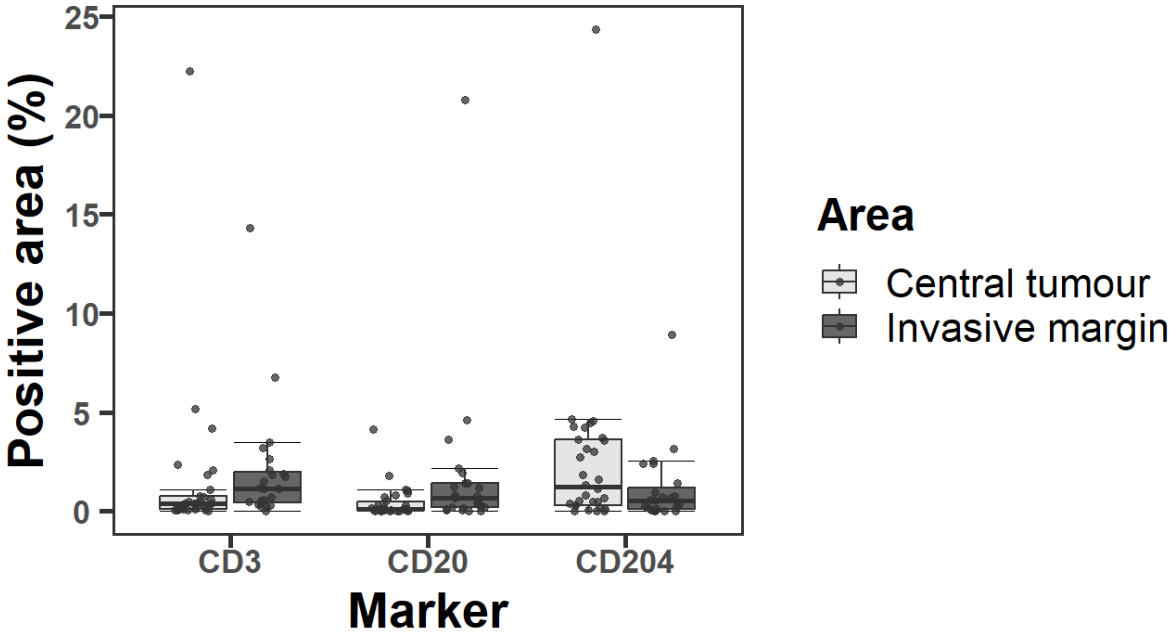

Figure 3.2 Comparison of CD3, CD20 and CD204 labelling between the central tumour (n=30) and invasive margin (n=23) areas for all tumours regardless of grade.

The invasive margin contained higher positive pixel percentages for CD3 and CD20 labelling than the central tumour. The central tumour contained a larger CD204 positive pixel percentage than the invasive margin.

Table 3.2 Wilcoxon signed-rank test results between central tumour and invasive margin.

Marker	Region	n	Median (%)	IQR (%)	p-value
CD20	CT	30	0.11	0.44	
	IM	23	0.65	1.25	0.008
CD3	CT	30	0.38	0.65	
	IM	23	1.16	1.57	0.014
FOXP3	CT	30	0.02	0.03	
	IM	23	0.05	0.12	0.006
Granzyme B	CT	30	0.02	0.01	
	IM	23	0.04	0.04	<0.001
CD204	CT	30	1.25	3.30	
	IM	23	0.54	1.10	0.055
CD206	CT	30	1.77	2.33	
	IM	23	1.44	1.47	0.377
FOXP3:CD3	CT	30	0.05	0.09	
	IM	23	0.06	0.08	0.742

Median, interquartile range (IQR) and p-Value between central tumour (CT) and invasive margin (IM) for the positive pixel percentages of CD20, CD3, FOXP3, Granzyme B, CD204, CD206 and FOXP3 to CD3 ratio.

A small number of outliers, present in the upper range, were observed both for the grade I and III tumours and for various markers, but especially for CD3, CD20 and CD204 (Figure 3.2).

3.1.2.2 Comparison of cellular infiltrates between high- and low-grade tumours in the central tumour area

Contrary to our hypothesis, there was no statistically significant difference in positive pixel percentages in the CT area for CD3, CD20, FOXP3, granzyme B, CD204 and CD206 markers between grade I and grade III tumours (Table 3.3). This suggests there is no significant difference in the number of T cells, B cells, T regs, combined CTL and NK cells, macrophages and specifically M2 macrophages between grade I and III tumours in the CT area of STS. Solely, for CD20 (B cells) a slight trend towards higher numbers of cells in central regions of grade I tumours compared to grade III tumours was observed.

Reflecting the comparison of CT and IM infiltrates in all tumours, the median CD204 positive pixel percentages in the CT also were significantly larger than the CD3 ($p=0.036$) and CD20 ($p<0.001$) positive pixel percentages both for grade I and III tumours (Figure 3.3and Table 3.3).

Generally (and in all markers except Granzyme B), the IQR was higher in the central tumour region of grade I tumours compared to grade III tumours (Table 3.3).

Table 3.3 Wilcoxon signed-rank test results between grade I and grade III tumours in the central tumour area.

Marker	Grade	n	Median (%)	IQR (%)	p-value
CD20	I	15	0.27	0.89	
	III	15	0.11	0.10	0.217
CD3	I	15	0.32	0.80	
	III	15	0.39	0.46	0.838
FOXP3	I	15	0.02	0.03	
	III	15	0.02	0.03	0.713
Granzyme B	I	15	0.01	0.01	
	III	15	0.04	0.05	0.539
CD204	I	15	1.16	3.28	
	III	15	1.33	3.07	0.935
CD206	I	15	2.21	2.85	
	III	15	1.74	1.92	0.902
FOXP3:CD3	I	15	0.05	0.09	
	III	15	0.04	0.09	0.836

Median, interquartile range (IQR) and p-Value between grade I and grade III tumours in the central tumour area for the positive pixel percentages of CD20, CD3, FOXP3, Granzyme B, CD204, CD206 and FOXP3 to CD3 ratio.

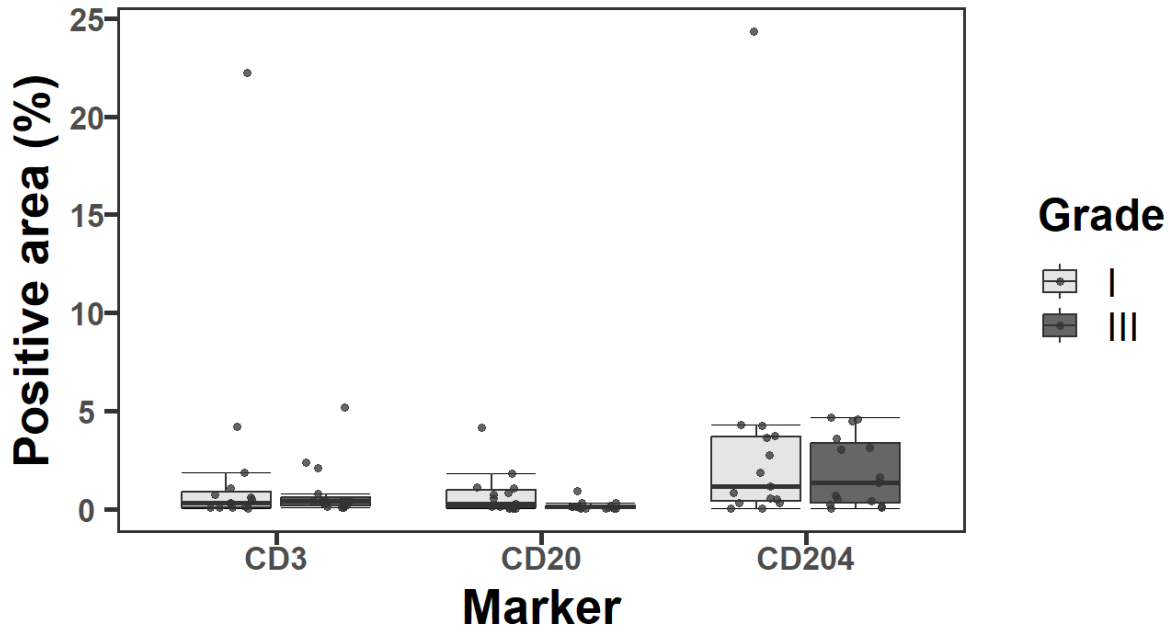

Figure 3.3 Comparison of CD3, CD20 and CD204 positive pixel percentages between grade I and grade III tumours in the central tumour area.

The central tumour had a higher percentage of CD204 positive pixels compared to CD3 and CD20 positive pixels. There was no significant difference between grade I and III tumours for each marker.

3.1.2.3 Comparison of cellular infiltrates between high- and low-grade tumours in the invasive margin area

Contrary to our hypothesis, there also was no statistically significant difference in positive pixel percentages in the IM area for CD3, CD20, FOXP3, granzyme B, CD204 and CD206 markers between grade I and grade III tumours (Figure 3.4and Table 3.4). This suggests there is no significant difference in the number of T cells, B cells, T regs, CTLs and NK cells, macrophages and specifically M2 macrophages between grade I and III tumours in the IM area of STS. For CD204 and FOXP3:CD3, there was a slight trend towards higher numbers for both parameters in grade I compared to grade III tumours. For granzyme B (CTLs and NK cells), there was a slight trend towards lower numbers in grade I compared to grade III tumours.

Reflecting on the comparison of CT and IM infiltrates in all tumours, the median CD204 positive pixel percentages in the IM also were smaller, yet not statistically significant, compared to the CD3 (p=0.055) and CD20 (p=0.513) positive pixel percentages both for grade I and III tumours (**Error! Reference source not found.** and Figure 3.4).

Similar to the central tumour regions, the IQR was higher in grade I tumours compared to grade III tumours for all markers except Granzyme B.

Table 3.4 Wilcoxon signed-rank test results between grade I and grade III tumours in the invasive margin area.

Marker	Grade	n	Median (%)	IQR (%)	p-value
CD20	I	12	0.61	1.27	
	III	11	0.65	1.23	0.833
CD3	I	12	0.86	1.71	
	III	11	1.19	1.33	0.880
FOXP3	I	12	0.06	0.22	
	III	11	0.05	0.07	0.740
Granzyme B	I	12	0.03	0.03	
	III	11	0.04	0.04	0.288
CD204	I	12	0.71	1.15	
	III	11	0.24	0.96	0.235
CD206	I	12	1.52	2.34	
	III	11	1.37	0.82	0.650
FOXP3:CD3	I	12	0.09	0.15	
	III	11	0.05	0.04	0.235

Median, interquartile range (IQR) and p-Value between grade I and grade III tumours in the invasive margin area for the positive pixel percentages of CD20, CD3, FOXP3, Granzyme B, CD204, CD206 and FOXP3 to CD3 ratio.

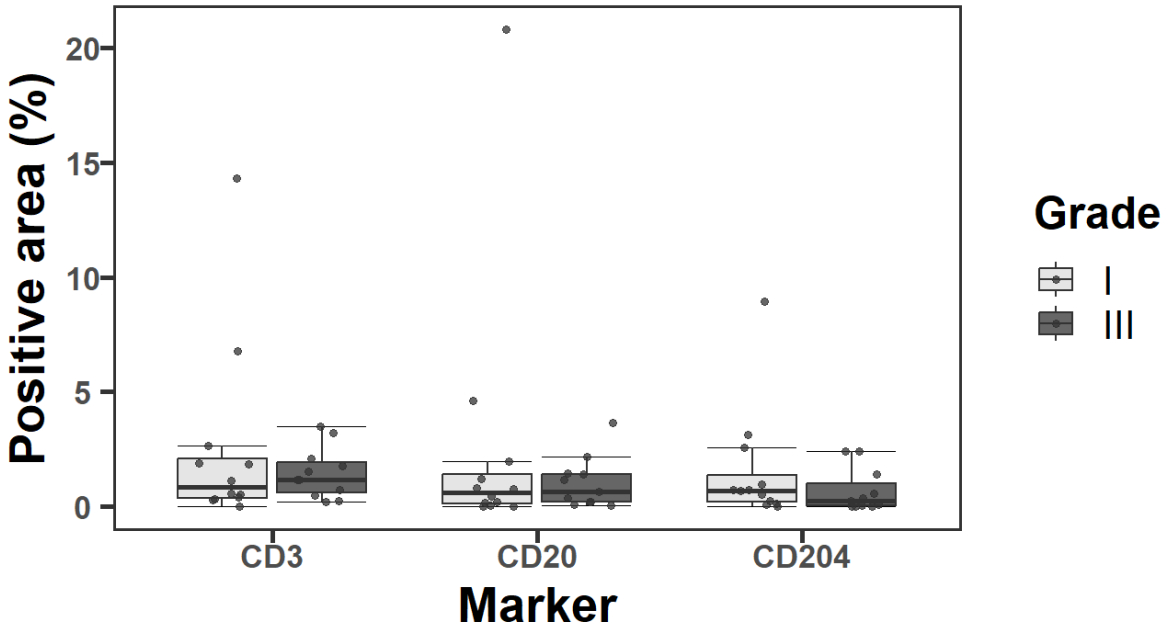

Figure 3.4 Comparison of CD3, CD20 and CD204 positive pixel percentages between the grade I and grade III tumours in the invasive margin area.

There was no significant difference between grade I and III tumours for CD3, CD20 and CD204 positive pixel percentages.

3.1.2.4 Comparison of cellular infiltrates with outcome data

Due to a lack of statistically significant differences between markers (and thus cellular populations) between grade I and grade III both for IM and CT regions and also the relatively low number of outcome data obtained, tumour samples from grades I and III were assessed combined.

In dogs for which the tumour recurred (5/15; five grade I, ten grade III), there were lower numbers of CD20, CD3, FOXP3, granzyme B and CD204 positively labelled cells and lower FOXP3 to CD3 ratio in the IM compared to dogs for which there was no recurrence. Additionally, dogs with local tumour recurrence also exhibited lower numbers of CD3, CD20, FOXP3, and granzyme B positively labelled cells, but higher numbers of CD206 positively labelled cells in the CT (Table 3.5).

Table 3.5 Presence of recurrence depending on the marker and area in the central tumour and invasive margin areas.

Marker	Recurrence	Central tumour			Invasive margin		
		n	Median (%)	IQR (%)	n	Median (%)	IQR (%)
CD20	Yes	5	0.049	0.036	3	0.047	0.702
	No	10	0.117	0.803	8	0.734	1.08
CD3	Yes	5	0.194	0.144	3	0.55	0.649
	No	10	0.400	1.16	8	1.15	0.694
FOXP3	Yes	5	0.013	0.014	3	0.006	0.019
	No	10	0.033	0.033	8	0.090	0.129
Granzyme B	Yes	5	0.010	0.005	3	0.025	0.003
	No	10	0.013	0.003	8	0.035	0.023
CD204	Yes	5	1.63	2.63	3	0.241	0.327
	No	10	0.921	3.33	8	0.304	1.10
CD206	Yes	5	2.47	3.1	3	1.04	1.50
	No	10	1.32	2.09	8	0.517	1.41
FOXP3:CD3	Yes	5	0.040	0.090	3	0.011	0.010
	No	10	0.039	0.062	8	0.064	0.034

IQR: Interquartile range.

In animals which developed distant metastasis after the surgery (4/9; 4 grade III) there were lower numbers of B cells, T cells, Tregs, CTLs and Granzyme B, macrophages, M2 macrophages, and a lower FOXP3 to CD3 ratio in the IM compared to dogs for which there was no distant metastasis. Additionally, such dogs also exhibited lower numbers of B cells, T cells, T regs, CTLs and NK cells, and a lower FOXP3 to CD3 ratio in the CT (Table 3.6).

Table 3.6 Presence of metastasis depending on the marker and area in the central tumour and invasive margin areas.

Marker	Metastasis	Central tumour			Invasive margin		
		n	Median (%)	IQR (%)	n	Median (%)	IQR (%)
CD20	Yes	4	0.078	0.078	4	0.159	0.235
	No	5	0.178	0.990	3	1.43	1.90
CD3	Yes	4	0.348	0.116	4	0.821	0.755
	No	5	0.415	3.81	3	1.14	6.78
FOXP3	Yes	4	0.006	0.017	4	0.041	0.046
	No	5	0.033	0.004	3	0.101	0.426
Granzyme B	Yes	4	0.009	0.008	4	0.027	0.012
	No	5	0.015	0.003	3	0.047	0.011
CD204	Yes	4	0.101	0.099	4	0.048	0.043
	No	5	4.30	3.14	3	3.15	4.28
CD206	Yes	4	1.14	3.52	4	1.02	1.24
	No	5	2.30	0.659	3	1.71	1.29
FOXP3:CD3	Yes	4	0.018	0.047	4	0.053	0.037
	No	5	0.078	0.065	3	0.064	0.013

IQR: Interquartile range.

In the dogs for which the cause of death was attributed to the tumour (6/14; two grade I, four grade III), there were lower numbers of B cells, T cells, Tregs,

CTLs and NKs, and macrophages in the IM compared to dogs that died of another cause. Additionally, such dogs also exhibited lower numbers of T cells, Tregs and macrophages in the CT, higher numbers of M2 macrophages in the IM, and both IM and CT exhibited a higher FOXP3 to CD3 ratio compared to dogs succumbing to death of other nature (Table 3.7).

Table 3.7 Outcome (death) depending on the marker and area in the central tumour and invasive margin areas.

Marker	Death caused by the tumour	Central tumour			Invasive margin		
		n	Median (%)	IQR (%)	n	Median (%)	IQR (%)
CD20	Yes	6	0.128	0.174	3	0.0473	0.368
	No	8	0.113	1.23	7	1.17	0.73
CD3	Yes	6	0.232	0.231	3	0.229	0.280
	No	8	1.13	2.25	7	1.78	1.61
FOXP3	Yes	6	0.025	0.014	3	0.008	0.114
	No	8	0.034	0.035	7	0.080	0.078
Granzyme B	Yes	6	0.011	0.009	3	0.022	0.093
	No	8	0.016	0.016	7	0.047	0.040
CD204	Yes	6	2.39	2.96	3	0.138	0.352
	No	8	3.92	3.1	7	2.42	2.18
CD206	Yes	6	2.34	1.81	3	1.58	0.596
	No	8	2.38	2.89	7	1.71	2.11
FOXP3:CD3	Yes	6	0.096	0.131	3	0.279	0.193
	No	8	0.029	0.029	7	0.063	0.044

IQR: Interquartile range.

3.2 Canine cutaneous histiocytoma

3.2.1 Sample population and clinical data

The sample population comprised 19 male (10 neutered and 9 entire) and 11 female (5 neutered and 6 entire) dogs of 18 different breeds. The age ranged from 0.4 to 12.8 years with a median of 2.4 years and IQR of 4.4 years. There were seven, eight, eight and seven group 1, 2, 3 and 4 cases, respectively. (Table 3.8).

Table 3.8 Clinical data for Histiocytoma cases.

Case	Breed	Sex	Age (years)	Histiocytoma group
1	Dalmatian	FE	2.7	1
2	Papillon	FE	1.6	1
3	French Bulldog	MN	1.2	2
4	Terrier	FE	10.4	1
5	Deerhound	MN	1.3	3
6	Golden Retriever	MN	6.8	2
7	Spaniel	ME	0.8	4
8	Cocker Spaniel	MN	7.1	4
9	Golden Retriever	FE	1.2	3
10	Crossbreed	ME	7.2	2
11	Spaniel	FN	4	3
12	Scottish Terrier	ME	6.2	1
13	Boxer	ME	3.5	2
14	Cocker Spaniel	MN	9	1
15	Spaniel	FN	2.7	3
16	Crossbreed	MN	1.3	4
17	French Bulldog	ME	0.7	4
18	Labradoodle	FN	2.5	4
19	Golden Retriever	MN	2.8	2
20	Rottweiler	MN	2.8	4
21	Terrier	MN	9	1
22	Spaniel	ME	0.7	2
23	Lurcher	FE	0.4	3
24	Husky	ME	2	3
25	Crossbreed	MN	2	2
26	Terrier	FN	2.2	1
27	Labrador	ME	0.9	4
28	English Springer Spaniel	ME	0.5	3
29	Golden Retriever	FE	1.7	2
30	Schnauzer	FN	12.8	3

FE : Female Entire. FN : Female Neutered. ME : Male Entire. MN : Male neutered.

3.2.2 Analysis of apoptosis, necrosis and immune cell infiltration

The outcome of the immunohistochemical staining revealed moderate to strong membranous staining and weak to moderate cytoplasmic staining for CD3 and CD204; weak to moderate to strong, cytoplasmic and nuclear staining for Active Caspase 3 and HMGB1 (Figure 3.5).

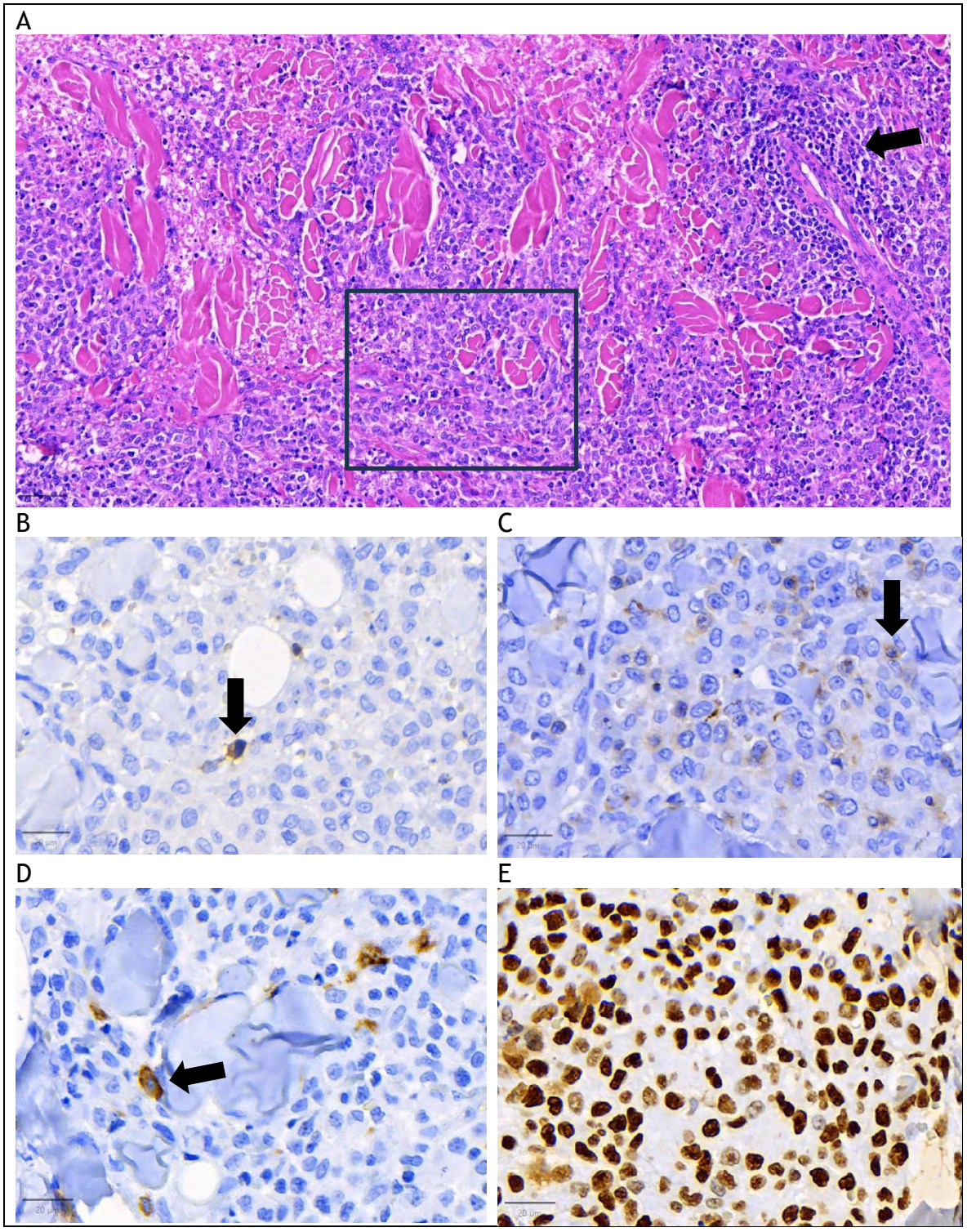

Figure 3.5 Histology and Immunohistochemistry of Canine Cutaneous Histiocytoma

A. Group 3 CCH with the presence of lymphocytic aggregates (black arrow). The rectangle represents the fields in B-E. CCH11, HE. Bar = 50 µm
B. Moderate cytoplasmic and weak nuclear staining (black arrow). CCH11, Active Caspase 3. Bar = 20 µm
C. Moderate membranous and weak cytoplasmic staining (black arrow). CCH11, CD3. Bar = 20 µm
D. Strong membranous and moderate cytoplasmic staining (black arrow). CCH11, CD204. Bar = 20 µm
E. Moderate to strong nuclear staining with mild to moderate cytoplasmic staining of all the cells. CCH11, HMGB1. Bar = 20 µm

Contrary to our hypothesis, the main cell death pathway highlighted in our study was apoptosis, as indicated by a statistically significant increase in positive pixel percentages of Active Caspase 3 over advanced progression (groups 1 to 4). In contrast to this, the HMGB1 positive cell areas, indicating necrosis or immunogenic cell death, decreased as regression increased, however, this finding was statistically not significant. At the same time, the IQR across the groups for HMGB1 positive cell areas and Active Caspase 3 also increased with the regression groups (Figure 3.6and Table 3.9) indicating greater variability between cases. These changes were accompanied by increasing numbers of T cells and macrophages with an advanced stage of regression, represented by a statistically significant increase in higher positive pixel percentages of CD3 and CD204 (Figure 3.6).

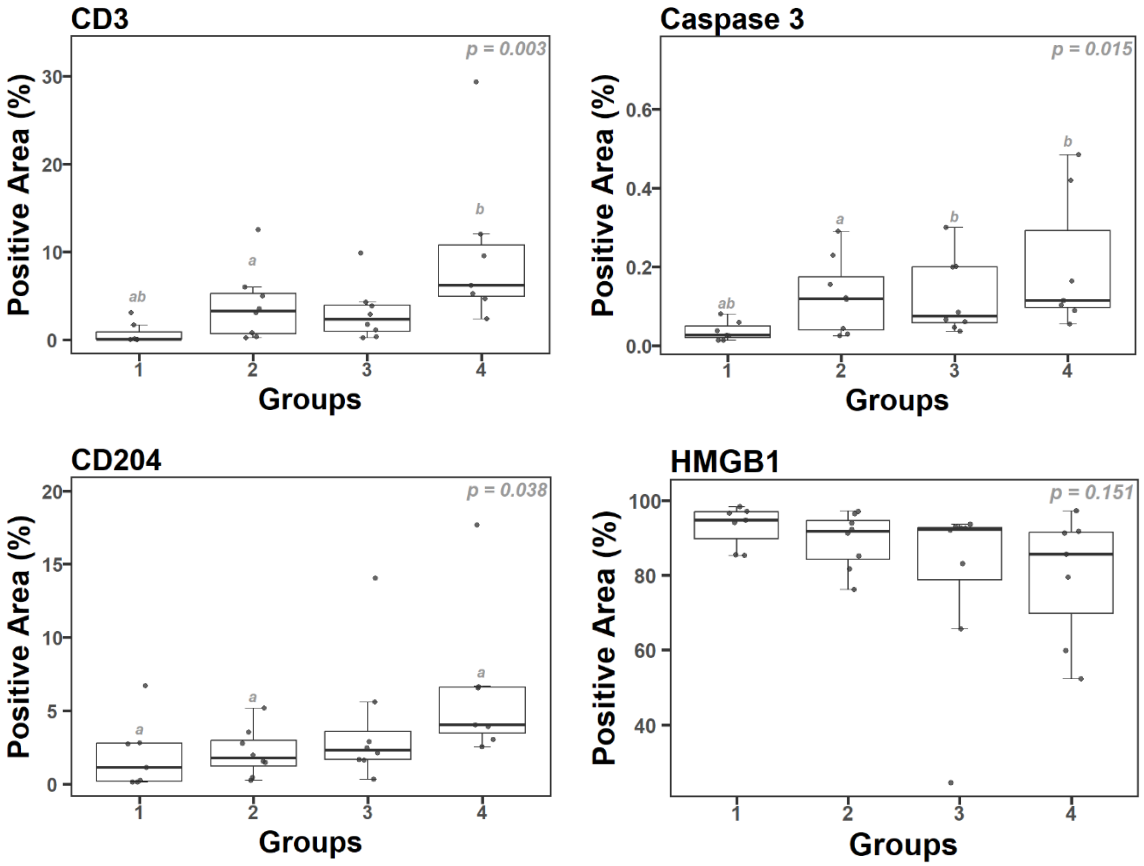

Figure 3.6 Boxplot of positive pixel percentages for CD3, Active Caspase 3 and CD204 and positive cell area percentages for HMGB1 in CCH regression groups.

The positive pixel percentages of CD3, Active Caspase 3 and CD204 increased across groups as regression progressed. At the same time, the HMGB1 positive cell area percentage decreased, but this change was not statistically significant. Superscript denotes where there are significant differences between groups (Dunn test for multiple comparisons).

Table 3.9 Kruskal-Wallis test results for positive pixel percentages of Caspase 3, CD3 and CD204 and positive cell area percentage of HMGB1.

Group	Median (%)	IQR (%)	p-Value
	Caspase 3 pixel area		
1	0.027[ab]	0.029	
2	0.119[a]	0.134	
3	0.075[b]	0.143	
4	0.115[b]	0.196	0.015
	CD3 pixel area		
1	0.036[ab]	0.866	
2	3.28[a]	4.57	
3	2.32	3	
4	6.21[b]	5.84	0.003
	CD204 pixel area		
1	1.15[a]	2.59	
2	1.78[a]	1.77	
3	2.32	1.91	
4	4.05[a]	3.13	0.038
	HMGB1 cellular area		
1	94.8	7.08	
2	91.9	10.3	
3	92.4	14	
4	85.7	21.8	0.151

Median, interquartile range (IQR) and p-Value of Kruskal-Wallis test for positive pixel percentages of Caspase 3, CD3 and CD204 and positive cell area percentage of HMGB1. Superscript denotes significant differences between groups, Dunn test for multiple comparisons. IQR: interquartile range.

Assessing the distribution pattern of HMGB1 in the cell more closely, the median of “DAB OD mean” in the cell, cytoplasm, nucleus and also the nuclear to cytoplasmic ratio progressively and subtly decreased across groups, except between groups 2 and 3 for the cellular and nuclear HMGB1 and between groups 1 and 2 for the nuclear to cytoplasmic ratio (Figure 3.7). However, none of these findings was statistically significant and also the IQR was very variable across groups (Table 3.10).

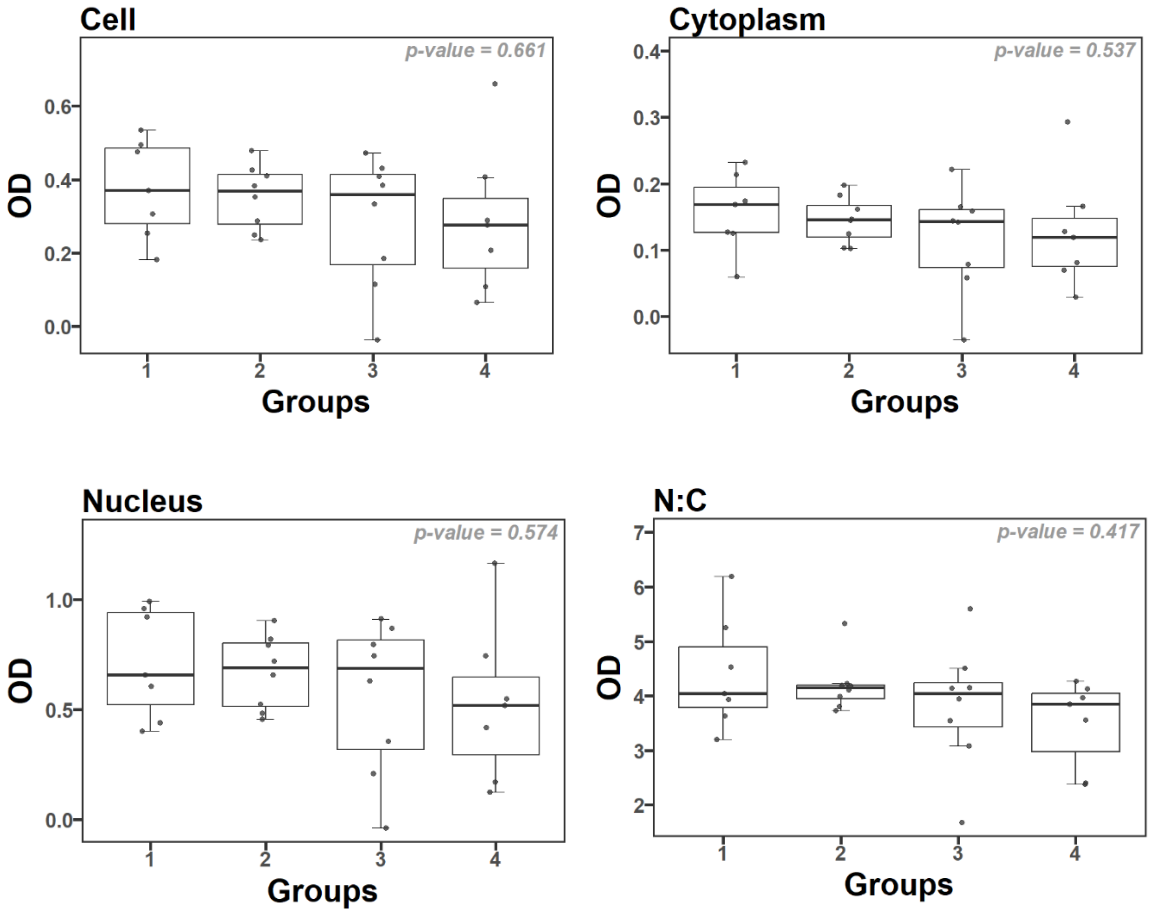

Figure 3.7 Boxplot of nuclear to cytoplasmic ratio (N :C), cellular, cytoplasmic and nuclear DAB OD of HMGB1 in CCH groups.

Whilst overall a subtle decrease was observed with tumour regression, the difference between groups was not statistically significant. OD: DAB optical density.

Table 3.10 Kruskal-Wallis test and ANOVA results for HMGB1

Group	Median (OD)	IQR (OD)	Mean (OD)	SD (OD)	p-Value
			Cytoplasmic HMGB1		
1	0.169	0.068	/	/	
2	0.145	0.0484	/	/	
3	0.143	0.0875	/	/	
4	0.119	0.0718	/	/	0.537*
			Nuclear HMGB1		
1	0.657	0.417	/	/	
2	0.689	0.287	/	/	
3	0.687	0.495	/	/	
4	0.518	0.351	/	/	0.574*
			N/C HMGB1		
1	4.04	1.11	/	/	
2	4.15	0.257	/	/	
3	4.04	0.804	/	/	
4	3.85	1.07	/	/	0.417*
			Cellular HMGB1		
1	/	/	0.393	0.201	
2	/	/	0.393	0.114	
3	/	/	0.398	0.247	
4	/	/	0.311	0.185	0.661**

Median, interquartile range (IQR) and p-Value of Kruskal-Wallis test (*) for HMGB1 cytoplasmic, nuclear and nuclear to cytoplasmic ratio median of DAB optical density. OD: DAB optical density. IQR: interquartile range. /: Not applicable. Median, interquartile range (IQR) and p-Value of ANOVA test (**) for cellular HMGB1 median of DAB optical density. OD: DAB optical density. IQR: interquartile range.

4 Discussion

4.1 Canine cutaneous and subcutaneous soft tissue sarcomas

The STS study identified three main findings. Firstly, using pixel areas values of the respective immunohistochemical markers to infer cell population numbers, there were generally higher numbers of B cells, T cells, Tregs and joint CTLs and NK cells in the IM when compared to the CT. In contrast to this, and (narrowly) only representing a tendency, there were higher numbers of macrophages in the CT when compared to the IM. Secondly, there was no difference in the number of TILs and TAMs, including particular cell populations previously associated with favourable tumour prognosis such as joint NK and cytotoxic T cells or macrophages, between grade I and grade III tumours. Thirdly, and reflecting the expectation of certain cell populations associated with a favourable prognosis, more B cells, T cells, CTLs and NKs were observed in the IM of animals with a better clinical outcome. However, and contrary to expected, T regs and macrophages were also higher in number in the IM of animals which had a better clinical outcome. Examination of the CT regions revealed less consistent associations.

4.1.1 Comparison between invasive margin and central tumour

Image and subsequent statistical analysis of the STS samples highlighted an increase of B cells, T cells, Tregs, and combined CTL and NK cells, i.e. all representing lymphocytes, in the IM compared to the CT region. Whilst corresponding investigations are lacking in the veterinary literature, similar findings have been reported for human tumours, including melanomas where TILs were assessed on H&E and with CD3 (T cell) and CD8 (CTL) markers (Mastracci et al. 2020), carcinomas of head and neck, kidney, pancreas and non-small-cell lung carcinoma where assessments were conducted with a CD8 marker (Steele et al. 2018), and breast cancer with CD3, CD8 and FOXP3 (Treg) markers (Miyan et al. 2016). Increased numbers of TILs in the IM compared to the CT have been shown to predict a better response to CTLA immune checkpoint inhibitors in human melanoma (Tumeh et al. 2014). The cause of the higher number of lymphocytes and their subtypes observed in the IM, when compared

to the CT, is unclear. However, it is suspected that the initial immune response to the tumour takes place in this area (Mastracci et al. 2020), which could explain higher numbers of immune cells in this region and cells decreasing towards the CT regions.

Interestingly, the CT tended to contain higher numbers of macrophages than the IM in the canine STSs under investigation. The reason for this is unknown. It may need to be hypothesized that this phenomenon represents the consequence of a different cytokine microenvironment between these two tumour areas. Regardless of the cause of this, studies examining human non-small-cell lung carcinoma have demonstrated that the spatial density and distribution of TAM subsets can represent independent predictors. Thus, lower numbers of M1 macrophages in the IM are associated with a worse prognosis, especially when the M2 macrophages are closely associated with the neoplastic cells (Zheng et al. 2020). However, the spatial density and distribution of the TIL and TAM subsets and their direct relationship with the neoplastic cells could potentially be of a prognostic interest and needs to be further investigated.

Finally, the IQR of lymphocyte-associated positive pixel areas was quite obviously higher in the IM compared to the CT. Similar findings have been reported in human tumours (Mastracci et al. 2020), however, the cause and clinical significance of this observation is unclear. One potential explanation could be that, with canine STSs representing a heterogenous group of tumours, the tumour population in this study likely captures different subtypes. Recent work has shown that the various subtypes of canine STSs may exhibit different TIL densities, and a higher IQR for CD3, CD20 and the FOXP3 to CD3 ratio has been reported depending on the grade and subtype of tumour (Avallone et al. 2024).

4.1.2 Comparison with the grade

The second main finding, and contrary to our hypothesis, was the lack of statistically significant difference between grade I and grade III tumours for all cell populations and markers investigated. Two studies conducted on canine STSs report similar findings for TILs when investigated with IHC markers against CD20, CD3 and FOXP3 (Avallone et al. 2024), and CD3, CD8, CD20 and FOXP3 (Nururrozi

et al. 2024). In contrast to this, human STSs show a significantly increased number of general T cells in grade III tumours compared to grade I or II tumours, whereas specific TIL subsets investigated, CTLs and Tregs, do not appear to vary significantly between grades (Smolle et al. 2021).

A study investigating TAMs in canine STS with the IHC marker Iba1 reports higher numbers of TAMs in grade III compared to grade I canine STSs (Finotello et al. 2021). The discrepancy to the current study, where no difference in CD204 (general macrophage) positive pixels and specifically CD206 (M2 macrophage) positive pixels were observed between grade I and grade III tumours, may reflect the use of a different IHC marker to investigate macrophages. Iba1 labels all histiocytic cells, including macrophages, Langerhans cells and interstitial dendritic cells (Pierezan et al. 2014), whereas CD204 is reported to be a more specific marker for macrophages only (Belluco et al. 2020, Kato et al. 2013, Kerboeuf et al. 2024, Seung et al. 2018). In addition, different methodologies were used in the two different studies to assess TAMs. In the present study, positive pixels were counted in the entire tumour, excluding necrotic areas, whereas Finotello *et al* counted cells in 10 high power field hotspots, excluding necrotic areas and other inflammatory cells (Finotello et al. 2021).

Interestingly, the present study showed greater CD206 areas compared to CD204 areas. CD206 is reported to represent a marker for M2 macrophages (Heinrich et al. 2017, Kerboeuf et al. 2024, Monteiro et al. 2018), whilst CD204 would be expected to stain the general macrophage population including M2 macrophages. A similar observation has also been reported previously in studies in canine hemangiosarcomas (Kerboeuf et al. 2024). Hypothetically, this could be the consequence of CD206 expression by resident Langerhans cells located in the dermis, a cell type that does not express CD204 but can express CD206 (Belluco et al. 2020), however, staining artefact may potentially need to be considered with either one marker, CD204, is not sensitive enough or the other marker, CD206, is exhibiting aberrant staining. Thus, dual immunolabelling for CD204 and CD206 should be performed to further elucidate this puzzling result and assess the true presence of M2 macrophages.

4.1.3 Comparison with the outcome data

Combining tissue analysis with outcome data, which to date lack comparable examinations in the veterinary field, indicated there were more B cells, T cells, CTLs and NKs in the IM of animals with a better clinical outcome. However, contrary to what was expected, T regs and macrophages were also higher in number in the IM of animals which had a better clinical outcome. Examination of the CT regions revealed less consistent associations.

Although not investigated with a logistic regression model due to the small data sets in this study, these findings support our initial hypothesis that infiltration by greater numbers of lymphocytes should have a positive effect on the clinical outcome. Beyond this, it appears that examination of the IM may be more valuable than focussing on the CT when assessing the inflammatory infiltrates in tumours and here in particular the TILs. However, these results are not supported by statistical analysis and further studies involving a greater sample population combined with a logistic regression analysis are required to make any more substantial conclusions on any prognostic indicators of survival, recurrence or metastasis and the impression that assessment of the IM might be more valuable than examination of the CT regions.

Interestingly, and contrary to our hypothesis, a higher Treg infiltration also appeared to have a positive influence on prognosis. Supporting the current findings are similar investigations in human STS that have shown low levels of FOXP3+ cells to be predictive of a poor survival, whereas a higher level of CD3+, CD4+ and FOXP3+ cells investigated by multiplex IHC was predictive of recurrence (Smolle et al. 2021). Such investigations have not been conducted in dogs and further multiplex IHC with combined CD3, CD20 and FOXP3 should be performed to enable a more thorough comparison with the findings reported in humans. A further explanation for the discrepant result may be that FOXP3 has been reported to also be expressed by effector CD4+ and CD8+ T cells in humans, thus FOXP3 labelling may not always be specific of Tregs (deLeeuw et al. 2012, Smolle et al. 2021). In addition, the immunosuppressive function of Tregs has been described to vary as they can exhibit a range of suppressive to non-suppressive functions depending on the relative expression of FOXP3 and CD45RA (Miyara et al. 2009). Consequently, further research on Tregs of dogs is

warranted, including their IHC markers and also to interpret the relationship of Tregs with neoplastic cells and their true immunosuppressive function.

4.1.4 Limitations

The STS study has several limitations.

The sample population derived from the SAH, a referral hospital, which receives more complex cases compared to the cases seen in general practices and thus may not be entirely representative of the general STS population. In addition, there were differences in the clinical presentation as some cases represented tumours localized on the head and in the perineal region, thus complicating resection and increasing the risk of incomplete or close margins, and of recurrence (McSporran 2009). The sample population was overrepresented by male dogs and, since other studies have not shown a sex predilection for canine STSs (Bray et al. 2014, Miyanishi et al. 2023, Nururrozi et al. 2024, Perry et al. 2014), this likely represents a sampling bias. Similarly, and consistent with sampling bias, PWT were overrepresented in grade I tumours whereas grade III tumours were overrepresented by undifferentiated sarcomas. In addition, and considering the entire dataset, PWT and undifferentiated tumours were overrepresented compared to PNST and fibrosarcoma. The study did not include any pleomorphic sarcomas or mesenchymomas. These elements are consistent with sampling bias. Additionally, the tumours were categorized by examining HE stained sections and IHC is often required to differentiate between subtypes of STS, especially to discriminate between PWT and PNST (Avallone et al. 2024, Avallone et al. 2007, Chijiwa et al. 2004, Dennis et al. 2011). Moreover, the presence or absence of clear/incomplete surgical margins was not taken into account, this may have also influenced the survival results.

Furthermore, the overall sample population was relatively small, which may have impeded the power of the statistical analysis especially when taking into account the presence of outliers which in turn may have skewed our results.

Whilst regular sampling of neoplastic specimen for histology by one cross- and two quarter sections contains an inherent sampling bias, a further bias may have been introduced at the point of FFPE tissue selection, when only one tissue

section per tumour was selected which in turn was based on the subjectively highest lymphocyte count and as little necrosis as possible. Additionally, selection of blocks according to these criteria did not allow assessment of the IM in all the cases, reducing the number of sections analysed and the statistical power of the results. The absence of a distinct IM on 7 sections may also have led to rejection of the hypothesis that there could be a difference in total and M2 macrophages between the CT and IM (type II statistical error).

The image analysis of the tumours also had several limitations. Firstly, the training dataset and study dataset were the same and generated by only one person (SK), thus the algorithms generated are expected to work fully only the dataset of this study. A bias due to the operator (SK) generating the algorithm cannot be excluded. However, as the same algorithm was applied to all the sections for a given stain, it is anticipated this bias is of minor significance. Secondly, selection of the tumour area was not straightforward, especially for invasive and poorly demarcated tumours and could thus have introduced a random selection bias. Thirdly, QuPath could not differentiate melanin, haemosiderin and lipofuscin pigments from true DAB labelling, however examination of the negative controls revealed only a small amount of these pigments to be present in the sections under investigation which could have, nevertheless, introduced a minor random bias. Similarly, in sections with substantial background and non-specific immunolabelling, QuPath was unable to differentiate between the background or non-specific immunolabelling and true immunolabeling; thus, all efforts to standardise the staining were made by carrying out the staining for one stain of all sections in the same run and therefore achieving comparable background and non-specific immunolabeling for all sections of one marker. The large interquartile range may also represent, in addition to the presence of an heterogenous subpopulation of STS tumours, an unreliable methodology which may need to be compared with another method of assessment of the positive areas (e.g. manual count on randomly selected areas). Finally, the immune cell infiltrates were assessed by counting pixels and not cells which may limit comparisons to other studies, but – since it represents an inherent bias – should not have an effect on the study results per se.

4.2 Canine cutaneous histiocytomas

The CCH study identified four main findings. Firstly, T cell numbers increased with regression, thus objectively validating the methodology used in this study. Secondly, we observed that apoptosis, indicated by an increase in Active Caspase 3, increased across groups. Thirdly, there also was an increase in the number of infiltrating macrophages across groups and fourthly, the overall presence of HMGB1 positive pixels, in turn representing a DAMP, an indicator of immunogenic cell death, was not significantly modified across groups.

4.2.1 Increased T-cell numbers across groups

The increased number of T cells across regression groups corresponds with published data (Belluco et al. 2020, Pires et al. 2013b). Thus, this objectively validates the methodology for dividing the masses into the 4 different regression groups applied in this study and at the same time also validates the use of the machine-learning process applied in this study. As demonstrated by Moore *et al,* most of the infiltrating T cells in CCH are CD8+ CTLs, which have capacity to induce apoptosis upon activation (Moore et al. 1996).

4.2.2 Apoptosis across groups

Immunolabeling for Active Caspase 3 increased across regression groups, indicating an increase in apoptosis with the regression stage. This correlates with recent publications demonstrating similar findings using IHC to detect Active Caspase 3, also by using QuPath on randomly selected areas and quantifying cytoplasmic immunolabelling with the cell detection function (Diehl and Hansmann 2024), or by performing matrix-assisted laser desorption/ionization mass spectrometry imaging and detecting increased peptides associated with apoptosis across groups (Loriani Fard et al. 2024). Interestingly, earlier work on apoptosis in CCH did not show any substantial difference between regression groups with the TUNEL assay (Kaim et al. 2006, Pires et al. 2013a). This may be due to non-specific labelling of cells with the TUNEL assay which also labels cells undergoing necroptosis, ferroptosis, pyroptosis and accidental cell death (Santagostino et al. 2021).

4.2.3 Macrophage infiltration across groups

The number of CD204 positive pixels, and by inference the number of macrophages, increased across regression groups. These findings corresponds to what has been reported in a study investigating macrophages with IHC for MAC387 and expression of iNOS RNA (Kaim et al. 2006). However, another study concluded that the extent of infiltrating macrophages was not statistically different across regression groups with IHC for MAC387 (Pires et al. 2013b). This discrepancy may represent differences in methodology to assess the positive cells as one study used a semi-quantitative method to assess the population of positive cells (Pires et al. 2013b), while the other quantitively evaluated the positive cell density per mm^2 (Kaim et al. 2006).

Nonetheless, the presence of infiltrating macrophages suggests an inflammatory response (Kaim et al. 2006), a finding not generally associated with apoptosis, as it is, at least historically, generally considered to be immunologically silent (Green et al. 2009, Oakes 2020). More recent work, by contrast, has shown apoptosis may elicit an inflammatory response in certain conditions, involving a complex interplay between dendritic cells, the release of DAMPs (such as HMGB1) and antigens of endogenous (e.g. neoplastic antigens) or exogenous origin (e.g. viral antigens) (Galluzzi et al. 2018, Green et al. 2009, Yatim et al. 2017). Hence, further and more detailed investigations of other regulated cell death pathways, such as necroptosis, pyroptosis and ferroptosis are warranted to improve our understanding of the inciting cause of inflammation in the regression of CCHs and further assess the presence of ICD in histiocytoma cells (Santagostino et al. 2021). These could be combined with extended evaluation of DAMPs released from neoplastic cells, and potentially also closely associated TME cells, ideally including double-staining to more adequately determine the source of DAMPs.

4.2.4 HMGB1 expression and location across groups

Contrary to our initial hypothesis, the presence of cytoplasmic, nuclear and cellular (combined nuclear and cytoplasmic) and the N:C ratio of HMGB1 did not significantly vary across groups, and overall, a very subtle decrease of HMGB1 unexpectedly involving all locations was observed over the course of CCH

regression. Nonetheless, there was clear evidence of localization of HMGB1 in the cytoplasm, in addition to variation of nuclear and cytoplasmic HMGB1 labelling and N:C ratio labelling in all the groups. The combination of these findings (i.e. concomitant decrease of HMGB1 labelling in both nucleus and cytoplasm) could represent individual cell DAMP release from the nucleus into the cytoplasm and extracellular space, in turn inducing chemotaxis and activation of various immune and inflammatory cells, including the macrophages observed to increase over CCH regression. Alternatively, and whilst it is unclear whether the IHC marker applied in this study binds both acetylated and non-acetylated HMGB1, canine macrophages and monocytes are reported to transfer acetylated-HMGB1 into their cytoplasm and then into the extracellular environment (Gardella et al. 2002, Sterenczak et al. 2011), which in the context of CCH regression and the ensuing reactive inflammatory response may have contributed to the changes in HMGB1 levels observed.

Interestingly, extracellular HMGB1, secreted by monocytes and macrophages or by necrotic cells, has been shown to activate dendritic cells by binding the receptor for advanced glycation end products (RAGE) and to induce dendritic cell maturation (Dumitriu et al. 2007, Manfredi et al. 2008, Yang et al. 2007). However, whether this includes specifically the Langerhans dendritic cells, i.e. the neoplastic population in CCH, is unclear. Considering the hypothesis of CCH regression mediated by histiocytoma cell maturation (Belluco et al. 2020, Loriani Fard et al. 2024, Pazdzior-Czapula et al. 2014, Pires et al. 2009, Pires et al. 2013b) and cytoplasmic expression of HMGB1 observed in the CCH study, it could be possible that binding of HMGB1 to RAGE receptors on Langerhans dendritic cells may contribute to Langerhans cell maturation and to regression. Further research on RAGE activation in histiocytoma/Langerhans dendritic cells and their maturation may shed more light on the significance of this finding.

Finally, IHC investigations in CCH have reported a variation between deep, central and superficial areas in the expression of CD208, CD206, Iba1 (Belluco et al. 2020), and E-cadherin IHC immunolabelling (Pires et al. 2009). Additionally, the immunolabelling pattern of some markers, such as MHCII, can vary between the deep, centre and superficial areas across groups (Pires et al. 2013b). Thus, further research investigating the spatial distribution of the IHC markers used in

this study, and especially HMGB1, may reveal more in-depth knowledge of the mechanisms leading to and accompanying CCH regression.

4.2.5 Limitations

The CCH study has several limitations. Firstly, the training dataset and study dataset were the same, thus the algorithms generated are expected to work fully only with the dataset of this study.

The grouping of CCH published by Cockerell *et al* (Cockerell and Slauson 1979) may be subjective and no studies have investigated intra- and inter-observer variation when using this grouping system. However, the relatively consistent increase of T cells quantitatively observed over regression groups in this study does support the possibility of a reliable application of the grouping system, which is typically done qualitatively, also in the present study.

Similar to the STS study, the sample population was overrepresented by male dogs whilst no sex predilection to CCH has been reported previously (Diehl and Hansmann 2024, Moore 2014). This may represent a sampling bias. Furthermore, the overall sample population was relatively small and each CCH group were also small. It may have impeded the power of the statistical analysis especially when considering the presence of outliers which in turn may have skewed our results.

Whilst regular sampling of neoplastic specimen for histology by one cross- and two quarter sections contains an inherent sampling bias, a further bias may have been introduced at the point of FFPE tissue selection, when only one tissue section per tumour was selected which in turn was based on the largest surface area and the least amount of crush artefact.

Regarding limitations at the quantification steps, it is unknown whether the cells expressing HMGB1 and Active Caspase 3 are neoplastic cells, part of the cellular component of the TME such as infiltrating macrophages that have a morphology which is indistinguishable from histiocytoma cells, or a combination of these. Therefore, also as briefly discussed above in regard to HMGB1, it may need to be considered whether the HMGB1 and Active Caspase 3 results may represent an average of a combination of neoplastic cells and TME cells rather than labelling

of the neoplastic cells alone. Specifically, in regard to the anti-HMGB1 antibody, the canine positive control tissues in our study also showed absent to only weak nuclear immunolabelling in smooth muscle cells, yet a strong nuclear immunolabelling in histiocytoma cells, keratinocytes and hepatocytes. Thus, it may need to be considered whether the nuclear, and consequently also the cytoplasmic, HMGB1 concentration and expression may vary amongst cell types and tissues. This should be taken into consideration in further studies, and could for example be investigated by quantifying HMGB1 in combination with double-immunolabelling in a range of normal tissue types.

Regarding QuPath, the limitations are the same as the ones stated in the STS study. Specifically, QuPath could not differentiate pigments (melanin, haemosiderin and lipofuscin) from true immunolabeling and could not differentiate between the background or non-specific immunolabelling and true immunolabeling. Similar to the STS study, this was mitigated by carrying out the staining for one stain of all sections. Thus, all efforts to standardise the staining were made by carrying out the staining for one stain of all sections in the same run and therefore achieving comparable background and non-specific immunolabeling for all sections of one marker. Lastly, the positive labelling was assessed by counting pixels and not cells, also limiting comparisons to other studies but it should not influence the study itself.

5 Conclusion

Despite several limitations, both studies conducted allowed to investigate and partially validate the use of artificial intelligence, in the form of QuPath, as a tool to investigate the immune environment in canine cutaneous and subcutaneous STSs and CCH. The lack of statistically significant differences observed between grade I and III canine cutaneous and subcutaneous STSs for all the marker used and also the statistically significant increase in T cells noted in the CCH study both correspond to previously published reports, thus supporting our use of QuPath as a reliable tool to investigate the immune environment in both these tumours.

In canine cutaneous and subcutaneous STSs, the area of tumour investigated (IM or CT) appeared to have an influence on the extent of the immune infiltrate in the neoplasms and dogs with a better clinical outcome exhibited increased numbers of B cells, T cells, Tregs and combined cytotoxic T cells and NK cells specifically in the IM. Further research should take into account the spatial distribution of the immune infiltrate of canine cutaneous and subcutaneous STSs, potentially also including and comparing a number of different STSs subtypes. Investigations on a larger population group, with standardized collection of outcome data, in addition to the research of expression of immune checkpoint inhibitors may help shed some light on potential prognostic markers and candidates for novel therapies.

The study on CCH highlighted the central role of apoptosis throughout the regression process, accompanied by infiltration of T cells and macrophages. However, the inciting event causing regression and also causing the striking inflammatory histiocytic inflammatory response despite the presence of apoptosis remains unclear. Further research on other mechanisms of cell death beyond apoptosis and necrosis, drivers of the immune response and neoplastic Langerhans cell maturation are warranted.

Bibliography

Ahmed, Z., Shaw, G., Sharma, V. P., Yang, C., McGowan, E. and Dickson, D. W. (2007) Actin-binding proteins coronin-1a and IBA-1 are effective microglial markers for immunohistochemistry. *J Histochem Cytochem, 55*(7), pp. 687–700.

Anderson, N. M. and Simon, M. C. (2020) The tumor microenvironment. *Curr Biol, 30*(16), pp. R921–R925.

Arimoto, K. I., Miyauchi, S., Liu, M. and Zhang, D. E. (2024) Emerging role of immunogenic cell death in cancer immunotherapy. *Front Immunol, 15*, pp. 1390263.

Avallone, G., Brigandi, E., Tugnoli, C., Rigillo, A., Bacci, B. and Roccabianca, P. (2024) Tumor-infiltrating lymphocytes vary in different canine soft tissue sarcoma histological types. *Vet Pathol*, pp. 3009858241300556.

Avallone, G., Helmbold, P., Caniatti, M., Stefanello, D., Nayak, R. C. and Roccabianca, P. (2007) The spectrum of canine cutaneous perivascular wall tumors: morphologic phenotypic and clinical characterization. *Veterinary Pathology, 44*(5), pp. 607–620.

Balkwill, F. R., Capasso, M. and Hagemann, T. (2012) The tumor microenvironment at a glance. *J Cell Sci, 125*(Pt 23), pp. 5591–6.

Bankhead, P., Loughrey, M. B., Fernandez, J. A., Dombrowski, Y., McArt, D. G., Dunne, P. D., McQuaid, S., Gray, R. T., Murray, L. J., Coleman, H. G., James, J. A., Salto-Tellez, M. and Hamilton, P. W. (2017) QuPath: Open source software for digital pathology image analysis. *Sci Rep, 7*(1), pp. 16878.

Barros, M. H., Hauck, F., Dreyer, J. H., Kempkes, B. and Niedobitek, G. (2013) Macrophage polarisation: an immunohistochemical approach for identifying M1 and M2 macrophages. *PLoS One, 8*(11), pp. e80908.

Belluco, S. (2018) Letter to the Editor. *Vet Pathol, 55*(4), pp. 597.

Belluco, S., Sammarco, A., Sapin, P., Lurier, T. and Marchal, T. (2020) FOXP3, CD208, and CD206 Expression in Canine Cutaneous Histiocytoma. *Vet Pathol, 57*(5), pp. 599–607.

Bertola, L., Pellizzoni, B., Giudice, C., Grieco, V., Ferrari, R., Chiti, L. E., Stefanello, D., Manfredi, M., De Zani, D. and Recordati, C. (2024) Tumor-associated macrophages and tumor-infiltrating lymphocytes in canine cutaneous and subcutaneous mast cell tumors. *Veterinary Pathology*.

Biller, B. J., Elmslie, R. E., Burnett, R. C., Avery, A. C. and Dow, S. W. (2007) Use of FoxP3 expression to identify regulatory T cells in healthy dogs and dogs with cancer. *Vet Immunol Immunopathol, 116*(1-2), pp. 69–78.

Boozer, L. B., Davis, T. W., Borst, L. B., Zseltvay, K. M., Olby, N. J. and Mariani, C. L. (2012) Characterization of immune cell infiltration into canine intracranial meningiomas. *Vet Pathol, 49*(5), pp. 784–95.

Boxberg, M., Leising, L., Steiger, K., Jesinghaus, M., Alkhamas, A., Mielke, M., Pfarr, N., Gotz, C., Wolff, K. D., Weichert, W. and Kolk, A. (2019) Composition and Clinical Impact of the Immunologic Tumor Microenvironment in Oral Squamous Cell Carcinoma. *J Immunol, 202*(1), pp. 278–291.

Bray, J. P. (2016) Soft tissue sarcoma in the dog - part 1: a current review. *J Small Anim Pract, 57*(10), pp. 510–519.

Bray, J. P., Polton, G. A., McSporran, K. D., Bridges, J. and Whitbread, T. M. (2014) Canine soft tissue sarcoma managed in first opinion practice: outcome in 350 cases. *Vet Surg, 43*(7), pp. 774–82.

Chijiwa, K., Uchida, K. and Tateyama, S. (2004) Immunohistochemical evaluation of canine peripheral nerve sheath tumors and other soft tissue sarcomas. *Veterinary Pathology, 41*(4), pp. 307–318.

Cockerell, G. L. and Slauson, D. O. (1979) Patterns of Lymphoid Infiltrate in the Canine Cutaneous Histiocytoma. *Journal of Comparative Pathology, 89*, pp. 193–203.

Collins, G. S., Ogundimu, E. O. and Altman, D. G. (2016) Sample size considerations for the external validation of a multivariable prognostic model: a resampling study. *Stat Med, 35*(2), pp. 214–26.

Costa, D., Ferreira, R., Prada, J., Queiroga, F. L., Rodrigues, P., Silva, F. and Pires, I. (2020) A Role for Angiogenesis in Canine Cutaneous Histiocytoma Regression: Insights into an Old Clinical Enigma. *In Vivo, 34*(6), pp. 3279–3284.

deLeeuw, R. J., Kost, S. E., Kakal, J. A. and Nelson, B. H. (2012) The prognostic value of FoxP3+ tumor-infiltrating lymphocytes in cancer: a critical review of the literature. *Clin Cancer Res, 18*(11), pp. 3022–9.

Dennis, M. M., McSporran, K. D., Bacon, N. J., Schulman, F. Y., Foster, R. A. and Powers, B. E. (2011) Prognostic factors for cutaneous and subcutaneous soft tissue sarcomas in dogs. *Vet Pathol, 48*(1), pp. 73–84.

Diehl, B. and Hansmann, F. (2024) Immune checkpoint regulation is critically involved in canine cutaneous histiocytoma regression. *Front Vet Sci, 11*, pp. 1371931.

Ducor, L., Fraga, M., Manco, R., Mdawar-Bailly, E., Vieira, J., Sempoux, C. and Moulin, P. (2026) Keratin 7 immunohistochemistry reveals patterns of cell populations in liver biopsies from patients with MASLD. *J Clin Pathol*.

Dumitriu, I. E., Bianchi, M. E., Bacci, M., Manfredi, A. A. and Rovere-Querini, P. (2007) The secretion of HMGB1 is required for the migration of maturing dendritic cells. *J Leukoc Biol, 81*(1), pp. 84–91.

Ettinger, S. N., Scase, T. J., Oberthaler, K. T., Craft, D. M., McKnight, J. A., Leibman, N. F., Charney, S. C. and Bergman, P. J. (2006) Association of argyrophilic nucleolar organizing regions, Ki-67, and proliferating cell nuclear antigen scores with histologic grade and survival in dogs with soft tissue sarcomas: 60 cases (1996-2002). *J Am Vet Med Assoc, 228*(7), pp. 1053–62.

Farhood, B., Najafi, M. and Mortezaee, K. (2019) CD8(+) cytotoxic T lymphocytes in cancer immunotherapy: A review. *J Cell Physiol, 234*(6), pp. 8509–8521.

Ferrer, L., Fondevila, D., Rabanal, R. and Ramis, A. (1992) Detection of T lymphocytes in canine tissue embedded in paraffin wax by means of antibody to CD3 antigen. *J Comp Pathol, 106*(3), pp. 311–4.

Finotello, R., Whybrow, K., Scarin, G. and Ressel, L. (2021) Correlation between Tumour Associated Macrophage (TAM) Infiltration and Mitotic Activity in Canine Soft Tissue Sarcomas. *Animals (Basel), 11*(3).

Fortuna, L., Relf, J., Chang, Y. M., Hibbert, A., Martineau, H. M. and Garden, O. A. (2016) Prevalence of FoxP3(+) Cells in Canine Tumours and Lymph Nodes Correlates Positively with Glucose Transporter 1 Expression. *J Comp Pathol, 155*(2-3), pp. 171–180.

Galluzzi, L., Aaronson, S. A., Abrams, J., Alnemri, E. S., Andrews, D. W., Baehrecke, E. H., Bazan, N. G., Blagosklonny, M. V., Blomgren, K., Borner, C., Bredesen, D. E., Brenner, C., Castedo, M., Cidlowski, J. A., Ciechanover, A., Cohen, G. M., De Laurenzi, V., De Maria, R., Deshmukh, M., Dynlacht, B. D., El-Deiry, W. S., Flavell, R. A., Fulda, S., Garrido, C., Golstein, P., Gougeon, M. L., Green, D. R., Gronemeyer, H., Hajnoczky, G., Hardwick, J. M., Hengartner, M. O., Ichijo, H., Jaattela, M., Kepp, O., Kimchi, A., Klionsky, D. J., Knight, R. A., Kornbluth, S., Kumar, S., Levine, B., Lipton, S. A., Lugli, E., Madeo, F., Malomi, W., Marine, J. C., Martin, S. J., Medema, J. P., Mehlen, P., Melino, G., Moll, U. M., Morselli, E., Nagata, S., Nicholson, D. W., Nicotera, P., Nunez, G., Oren, M., Penninger, J., Pervaiz, S., Peter, M. E., Piacentini, M., Prehn, J. H., Puthalakath, H., Rabinovich, G. A., Rizzuto, R., Rodrigues, C. M., Rubinsztein, D. C., Rudel, T., Scorrano, L., Simon, H. U., Steller, H., Tschopp, J., Tsujimoto, Y., Vandenabeele, P., Vitale, I., Vousden, K. H., Youle, R. J., Yuan, J., Zhivotovsky, B. and Kroemer, G. (2009) Guidelines for the use and interpretation of assays for monitoring cell death in higher eukaryotes. *Cell Death Differ, 16*(8), pp. 1093–107.

Galluzzi, L., Vitale, I., Aaronson, S. A., Abrams, J. M., Adam, D., Agostinis, P., Alnemri, E. S., Altucci, L., Amelio, I., Andrews, D. W., Annicchiarico-Petruzzelli, M., Antonov, A. V., Arama, E., Baehrecke, E. H., Barlev, N. A., Bazan, N. G., Bernassola, F., Bertrand, M. J. M., Bianchi, K., Blagosklonny, M. V., Blomgren, K., Borner, C., Boya, P., Brenner, C., Campanella, M., Candi, E., Carmona-Gutierrez, D., Cecconi, F., Chan, F. K., Chandel, N. S., Cheng, E. H., Chipuk, J. E., Cidlowski, J. A., Ciechanover, A., Cohen, G. M., Conrad, M., Cubillos-Ruiz, J. R., Czabotar, P. E., D'Angiolella, V., Dawson, T. M., Dawson, V. L., De Laurenzi, V., De Maria, R., Debatin, K. M., DeBerardinis, R. J., Deshmukh, M., Di Daniele,

N., Di Virgilio, F., Dixit, V. M., Dixon, S. J., Duckett, C. S., Dynlacht, B. D., El-Deiry, W. S., Elrod, J. W., Fimia, G. M., Fulda, S., Garcia-Saez, A. J., Garg, A. D., Garrido, C., Gavathiotis, E., Golstein, P., Gottlieb, E., Green, D. R., Greene, L. A., Gronemeyer, H., Gross, A., Hajnoczky, G., Hardwick, J. M., Harris, I. S., Hengartner, M. O., Hetz, C., Ichijo, H., Jaattela, M., Joseph, B., Jost, P. J., Juin, P. P., Kaiser, W. J., Karin, M., Kaufmann, T., Kepp, O., Kimchi, A., Kitsis, R. N., Klionsky, D. J., Knight, R. A., Kumar, S., Lee, S. W., Lemasters, J. J., Levine, B., Linkermann, A., Lipton, S. A., Lockshin, R. A., Lopez-Otin, C., Lowe, S. W., Luedde, T., Lugli, E., MacFarlane, M., Madeo, F., Malewicz, M., Malorni, W., Manic, G., Marine, J. C., Martin, S. J., Martinou, J. C., Medema, J. P., Mehlen, P., Meier, P., Melino, S., Miao, E. A., Molkentin, J. D., Moll, U. M., Munoz-Pinedo, C., Nagata, S., Nunez, G., Oberst, A., Oren, M., Overholtzer, M., Pagano, M., Panaretakis, T., Pasparakis, M., Penninger, J. M., Pereira, D. M., Pervaiz, S., Peter, M. E., Piacentini, M., Pinton, P., Prehn, J. H. M., Puthalakath, H., Rabinovich, G. A., Rehm, M., Rizzuto, R., Rodrigues, C. M. P., Rubinsztein, D. C., Rudel, T., Ryan, K. M., Sayan, E., Scorrano, L., Shao, F., Shi, Y., Silke, J., Simon, H. U., Sistigu, A., Stockwell, B. R., Strasser, A., Szabadkai, G., Tait, S. W. G., Tang, D., Tavernarakis, N., Thorburn, A., Tsujimoto, Y., Turk, B., Vanden Berghe, T., Vandenabeele, P., Vander Heiden, M. G., Villunger, A., Virgin, H. W., Vousden, K. H., Vucic, D., Wagner, E. F., Walczak, H., Wallach, D., Wang, Y., Wells, J. A., Wood, W., Yuan, J., Zakeri, Z., Zhivotovsky, B., Zitvogel, L., Melino, G. and Kroemer, G. (2018) Molecular mechanisms of cell death: recommendations of the Nomenclature Committee on Cell Death 2018. *Cell Death Differ, 25*(3), pp. 486–541.

Garcia, I., Martinou, I., Tsujimoto, Y. and Martinou, J. C. (1992) Prevention of programmed cell death of sympathetic neurons by the bcl-2 proto-oncogene. *Science, 258*(5080), pp. 302–4.

Gardella, S., Andrei, C., Ferrera, D., Lotti, L. V., Torrisi, M. R., Bianchi, M. E. and Rubartelli, A. (2002) The nuclear protein HMGB1 is secreted by monocytes via a non-classical, vesicle-mediated secretory pathway. *EMBO Rep, 3*(10), pp. 995–1001.

Giuliano, A., Pimentel, P. A. B. and Horta, R. S. (2024) Checkpoint Inhibitors in Dogs: Are We There Yet? *Cancers, 16*(11).

Glick, A. D., Holscher, M. and Campbell, G. R. (1976) Canine cutaneous histiocytoma: ultrastructural and cytochemical observations. *Vet Pathol, 13*(5), pp. 374–80.

Green, D. R., Ferguson, T., Zitvogel, L. and Kroemer, G. (2009) Immunogenic and tolerogenic cell death. *Nat Rev Immunol, 9*(5), pp. 353–63.

Guvenc, T., Haligur, M., Orman, M. N. and Haziroglu, R. (2002) Mitosis and apoptosis in canine cutaneous histiocytoma and transmissible venereal tumour. *Acta Vet Hung, 50*(3), pp. 315–21.

Han, J., Zhang, B., Zheng, S., Jiang, Y., Zhang, X. and Mao, K. (2024) The Progress and Prospects of Immune Cell Therapy for the Treatment of Cancer. *Cell Transplant, 33*, pp. 9636897241231892.

Heinrich, F., Lehmbecker, A., Raddatz, B. B., Kegler, K., Tipold, A., Stein, V. M., Kalkuhl, A., Deschl, U., Baumgartner, W., Ulrich, R. and Spitzbarth, I. (2017) Morphologic, phenotypic, and transcriptomic characterization of classically and alternatively activated canine blood-derived macrophages in vitro. *PLoS One, 12*(8), pp. e0183572.

Hendry, S., Salgado, R., Gevaert, T., Russell, P. A., John, T., Thapa, B., Christie, M., van de Vijver, K., Estrada, M. V., Gonzalez-Ericsson, P. I., Sanders, M., Solomon, B., Solinas, C., Van den Eynden, G., Allory, Y., Preusser, M., Hainfellner, J., Pruneri, G., Vingiani, A., Demaria, S., Symmans, F., Nuciforo, P., Comerma, L., Thompson, E. A., Lakhani, S., Kim, S. R., Schnitt, S., Colpaert, C., Sotiriou, C., Scherer, S. J., Ignatiadis, M., Badve, S., Pierce, R. H., Viale, G., Sirtaine, N., Penault-Llorca, F., Sugie, T., Fineberg, S., Paik, S., Srinivasan, A., Richardson, A., Wang, Y., Chmielik, E., Brock, J., Johnson, D. B., Balko, J., Wienert, S., Bossuyt, V., Michiels, S., Ternes, N., Burchardi, N., Luen, S. J., Savas, P., Klauschen, F., Watson, P. H., Nelson, B. H., Criscitiello, C., O'Toole, S., Larsimont, D., de Wind, R., Curigliano, G., Andre, F., Lacroix-Triki, M., van de Vijver, M., Rojo, F., Floris, G., Bedri, S., Sparano, J., Rimm, D., Nielsen, T., Kos, Z., Hewitt, S., Singh, B., Farshid, G., Loibl, S., Allison, K. H., Tung, N., Adams, S., Willard-Gallo, K., Horlings, H. M., Gandhi, L., Moreira, A., Hirsch, F., Dieci, M. V., Urbanowicz, M., Brcic, I., Korski, K., Gaire, F., Koeppen, H., Lo, A., Giltnane, J., Rebelatto, M. C., Steele, K. E., Zha, J., Emancipator, K., Juco, J. W., Denkert, C., Reis-Filho, J., Loi, S. and Fox, S. B. (2017a) Assessing Tumor-Infiltrating Lymphocytes in Solid Tumors: A Practical Review for Pathologists and Proposal for a Standardized Method from the International Immuno-Oncology Biomarkers Working Group: Part 2: TILs in Melanoma, Gastrointestinal Tract Carcinomas, Non-Small Cell Lung Carcinoma and Mesothelioma, Endometrial and Ovarian Carcinomas, Squamous Cell Carcinoma of the Head and Neck, Genitourinary Carcinomas, and Primary Brain Tumors. *Adv Anat Pathol, 24*(6), pp. 311–335.

Hendry, S., Salgado, R., Gevaert, T., Russell, P. A., John, T., Thapa, B., Christie, M., van de Vijver, K., Estrada, M. V., Gonzalez-Ericsson, P. I., Sanders, M., Solomon, B., Solinas, C., Van den Eynden, G., Allory, Y., Preusser, M., Hainfellner, J., Pruneri, G., Vingiani, A., Demaria, S., Symmans, F., Nuciforo, P., Comerma, L., Thompson, E. A., Lakhani, S., Kim, S. R., Schnitt, S., Colpaert, C., Sotiriou, C., Scherer, S. J., Ignatiadis, M., Badve, S., Pierce, R. H., Viale, G., Sirtaine, N., Penault-Llorca, F., Sugie, T., Fineberg, S., Paik, S., Srinivasan, A., Richardson, A., Wang, Y., Chmielik, E., Brock, J., Johnson, D. B., Balko, J., Wienert, S., Bossuyt, V., Michiels, S., Ternes, N., Burchardi, N., Luen, S. J., Savas, P., Klauschen, F., Watson, P. H., Nelson, B. H., Criscitiello, C., O'Toole, S., Larsimont, D., de Wind, R., Curigliano, G., Andre, F., Lacroix-Triki, M., van de Vijver, M., Rojo, F., Floris, G., Bedri, S., Sparano, J., Rimm, D., Nielsen, T., Kos, Z., Hewitt, S., Singh, B., Farshid, G., Loibl, S., Allison, K. H., Tung, N., Adams, S., Willard-Gallo, K., Horlings, H. M., Gandhi, L., Moreira, A., Hirsch, F., Dieci, M. V., Urbanowicz, M., Brcic, I., Korski, K., Gaire, F., Koeppen, H., Lo, A., Giltnane, J., Rebelatto, M. C., Steele, K. E., Zha, J., Emancipator, K., Juco, J. W., Denkert, C., Reis-Filho, J., Loi, S. and Fox, S. B. (2017b) Assessing Tumor-infiltrating Lymphocytes in Solid

Tumors: A Practical Review for Pathologists and Proposal for a Standardized Method From the International Immunooncology Biomarkers Working Group: Part 1: Assessing the Host Immune Response, TILs in Invasive Breast Carcinoma and Ductal Carcinoma In Situ, Metastatic Tumor Deposits and Areas for Further Research. *Adv Anat Pathol, 24*(5), pp. 235–251.

Humphries, M. P., Maxwell, P. and Salto-Tellez, M. (2021) QuPath: The global impact of an open source digital pathology system. *Comput Struct Biotechnol J, 19*, pp. 852–859.

Ito, D., Imai, Y., Ohsawa, K., Nakajima, K., Fukuuchi, Y. and Kohsaka, S. (1998) Microglia-specific localisation of a novel calcium binding protein, Iba1. *Brain Res Mol Brain Res, 57*(1), pp. 1–9.

Jain, R. K. (2013) Normalizing tumor microenvironment to treat cancer: bench to bedside to biomarkers. *J Clin Oncol, 31*(17), pp. 2205–18.

Jin, M. Z. and Jin, W. L. (2020) The updated landscape of tumor microenvironment and drug repurposing. *Signal Transduct Target Ther, 5*(1), pp. 166.

Jubala, C. M., Wojcieszyn, J. W., Valli, V. E., Getzy, D. M., Fosmire, S. P., Coffey, D., Bellgrau, D. and Modiano, J. F. (2005) CD20 expression in normal canine B cells and in canine non-Hodgkin lymphoma. *Vet Pathol, 42*(4), pp. 468–76.

Kaim, U., Moritz, A., Failing, K. and Baumgartner, W. (2006) The regression of a canine Langerhans cell tumour is associated with increased expression of IL-2, TNF-alpha, IFN-gamma and iNOS mRNA. *Immunology, 118*(4), pp. 472–82.

Kang, S., Penaloza Aponte, J. D., Elashkar, O., Morales, J. F., Waddington, N., Lamb, D. G., Ju, H., Campbell-Thompson, M. and Kim, S. (2025) Leveraging pre-trained machine learning models for islet quantification in type 1 diabetes. *J Pathol Inform, 16*, pp. 100406.

Kato, Y., Murakami, M., Hoshino, Y., Mori, T., Maruo, K., Hirata, A., Nakagawa, T. L., Yanai, T. and Sakai, H. (2013) The class A macrophage scavenger receptor CD204 is a useful immunohistochemical marker of canine histiocytic sarcoma. *J Comp Pathol, 148*(2-3), pp. 188–96.

Kelly, D. F. (1970) Canine cutaneous histiocytoma. A light and electron microscopic study. *Pathol Vet, 7*(1), pp. 12–27.

Kerboeuf, M., Haugeberg, D. A., Olsen, T., Sorling, L. K., Koppang, E. O., Moe, L. and Haaland, A. H. (2024) Tumor-associated macrophages in canine visceral hemangiosarcoma. *Vet Pathol, 61*(1), pp. 32–45.

Kerr, J. F., Wyllie, A. H. and Currie, A. R. (1972) Apoptosis: a basic biological phenomenon with wide-ranging implications in tissue kinetics. *Br J Cancer, 26*(4), pp. 239–57.

Krajewska, M., Wang, H. G., Krajewski, S., Zapata, J. M., Shabaik, A., Gascoyne, R. and Reed, J. C. (1997) Immunohistochemical analysis of in vivo patterns of expression of CPP32 (Caspase-3), a cell death protease. *Cancer Res, 57*(8), pp. 1605–13.

Oakes, S.A. (2020) 'Cell Injury, Cell Death, and Adaptations' In: Pathologic Basis of Disease, 10th edition (ed. R.Kumar, A.K.Abbas, J.C.Aster), Elsevier, 33-66.

Lane, L. V., Allison, R. W., Rizzi, T. R., Stern, A. W., Snider, T. A., Moore, P. F. and Vernau, W. (2012) Canine intravascular lymphoma with overt leukemia. *Vet Clin Pathol, 41*(1), pp. 84–91.

Lang, H. P., Osum, K. C. and Friedenberg, S. G. (2024) A review of CD4(+) T cell differentiation and diversity in dogs. *Vet Immunol Immunopathol, 275*, pp. 110816.

Laplane, L., Duluc, D., Larmonier, N., Pradeu, T. and Bikfalvi, A. (2018) The Multiple Layers of the Tumor Environment. *Trends Cancer, 4*(12), pp. 802–809.

Li, A., Pang, Y., Zhang, H., Wu, D., Lin, L., He, Z., Liang, Z., Chen, J. and Li, F. (2026) Automated quantification of tumor-infiltrating lymphocytes by machine learning reveals prognostic and immunogenomic features in lung cancer. *Sci Rep, 16*(1), pp. 7006.

Liu, J., Geng, X., Hou, J. and Wu, G. (2021) New insights into M1/M2 macrophages: key modulators in cancer progression. *Cancer Cell Int, 21*(1), pp. 389.

Liu, K., Xia, W., Qiang, M., Chen, X., Liu, J., Guo, X. and Lv, X. (2020) Deep learning pathological microscopic features in endemic nasopharyngeal cancer: Prognostic value and protentional role for individual induction chemotherapy. *Cancer Med, 9*(4), pp. 1298–1306.

Lopez-Janeiro, A., Padilla-Ansala, C., de Andrea, C. E., Hardisson, D. and Melero, I. (2020) Prognostic value of macrophage polarization markers in epithelial neoplasms and melanoma. A systematic review and meta-analysis. *Mod Pathol, 33*(8), pp. 1458–1465.

Loriani Fard, A. K., Haake, A., Jovanovic, V., Andreotti, S., Hummel, M., Hempel, B. F. and Gruber, A. D. (2024) Immuno-oncologic profiling by stage-dependent transcriptome and proteome analyses of spontaneously regressing canine cutaneous histiocytoma. *PeerJ, 12*, pp. e18444.

Maeda, S., Ohno, K., Fujiwara-Igarashi, A., Uchida, K. and Tsujimoto, H. (2016) Changes in Foxp3-Positive Regulatory T Cell Number in the Intestine of Dogs With Idiopathic Inflammatory Bowel Disease and Intestinal Lymphoma. *Vet Pathol, 53*(1), pp. 102–12.

Maman, S. and Witz, I. P. (2018) A history of exploring cancer in context. *Nat Rev Cancer, 18*(6), pp. 359–376.

Manfredi, A. A., Capobianco, A., Esposito, A., De Cobelli, F., Canu, T., Monno, A., Raucci, A., Sanvito, F., Doglioni, C., Nawroth, P. P., Bierhaus, A., Bianchi, M. E., Rovere-Querini, P. and Del Maschio, A. (2008) Maturing dendritic cells depend on RAGE for in vivo homing to lymph nodes. *J Immunol, 180*(4), pp. 2270–5.

Mao, X., Xu, J., Wang, W., Liang, C., Hua, J., Liu, J., Zhang, B., Meng, Q., Yu, X. and Shi, S. (2021) Crosstalk between cancer-associated fibroblasts and immune cells in the tumor microenvironment: new findings and future perspectives. *Mol Cancer, 20*(1), pp. 131.

Martin De Las Mulas, J., Millan, Y., Ruiz-Villamor, E. and Bautista, M. J. (1998) Apoptosis and mitosis in tumours of the skin and subcutaneous tissues of the dog. *Research in Veterinary Science, 66*, pp. 139–146.

Martinez, M. and Moon, E. K. (2019) CAR T Cells for Solid Tumors: New Strategies for Finding, Infiltrating, and Surviving in the Tumor Microenvironment. *Front Immunol, 10*, pp. 128.

Mastracci, L., Fontana, V., Queirolo, P., Carosio, R., Grillo, F., Morabito, A., Banelli, B., Tanda, E., Boutros, A., Dozin, B., Gualco, M., Salvi, S., Romani, M., Spagnolo, F., Poggi, A. and Pistillo, M. P. (2020) Response to ipilimumab therapy in metastatic melanoma patients: potential relevance of CTLA-4(+) tumor infiltrating lymphocytes and their in situ localization. *Cancer Immunol Immunother, 69*(4), pp. 653–662.

McSporran, K. D. (2009) Histologic grade predicts recurrence for marginally excised canine subcutaneous soft tissue sarcomas. *Vet Pathol, 46*(5), pp. 928–33.

Miller, M. A. and Zachary, J. F. (2017) Mechanisms and Morphology of Cellular Injury, Adaptation, and Death. in *Pathologic Basis of Veterinary Disease*. pp. 2–43.e19.

Miyan, M., Schmidt-Mende, J., Kiessling, R., Poschke, I. and de Boniface, J. (2016) Differential tumor infiltration by T-cells characterizes intrinsic molecular subtypes in breast cancer. *J Transl Med, 14*(1), pp. 227.

Miyanishi, K., Nururrozi, A., Igase, M., Tanabe, M., Sakurai, M., Sakai, Y., Shimonohara, N., Murakami, M. and Mizuno, T. (2023) Activation of the Akt signalling pathway as a prognostic indicator in canine soft tissue sarcoma. *J Comp Pathol, 206*, pp. 44–52.

Miyara, M., Yoshioka, Y., Kitoh, A., Shima, T., Wing, K., Niwa, A., Parizot, C., Taflin, C., Heike, T., Valeyre, D., Mathian, A., Nakahata, T., Yamaguchi, T., Nomura, T., Ono, M., Amoura, Z., Gorochov, G. and Sakaguchi, S. (2009) Functional delineation and differentiation dynamics of human CD4+ T cells expressing the FoxP3 transcription factor. *Immunity, 30*(6), pp. 899–911.

Mondal, R., Sandhu, Y. K., Kamalia, V. M., Delaney, B. A., Syed, A. U., Nguyen, G. A. H., Moran, T. R., Limpengco, R. R., Liang, C. and Mukherjee, J. (2023) Measurement of Abeta Amyloid Plaques and Tau Protein in

Postmortem Human Alzheimer's Disease Brain by Autoradiography Using [(18)F]Flotaza, [(125)I]IBETA, [(124/125)I]IPPI and Immunohistochemistry Analysis Using QuPath. *Biomedicines, 11*(4).

Monteiro, L. N., Rodrigues, M. A., Gomes, D. A., Salgado, B. S. and Cassali, G. D. (2018) Tumour-associated macrophages: Relation with progression and invasiveness, and assessment of M1/M2 macrophages in canine mammary tumours. *Vet J, 234*, pp. 119–125.

Moore, P., Schrenzel, M. D., Affolter, V., Olivry, T. and Naydan, D. (1996) Canine cutaneous histiocytoma is an epidermotropic Langerhans cell histiocytosis that expresses CD1 and specific beta 2-integrin molecules. *American Journal of Pathology, 148*(5), pp. 1699–1708.

Moore, P. F. (2014) A review of histiocytic diseases of dogs and cats. *Vet Pathol, 51*(1), pp. 167–84.

Moore, P. F. (2023) Histiocytic Diseases. *Vet Clin North Am Small Anim Pract, 53*(1), pp. 121–140.

Muscatello, L. V., Avallone, G., Brunetti, B., Bacci, B., Foschini, M. P. and Sarli, G. (2022) Standardized approach for evaluating tumor infiltrating lymphocytes in canine mammary carcinoma: Spatial distribution and score as relevant features of tumor malignancy. *Vet J, 283-284*, pp. 105833.

Newton, K., Strasser, A., Kayagaki, N. and Dixit, V. M. (2024) Cell death. *Cell, 187*(2), pp. 235–256.

Nururrozi, A., Miyanishi, K., Igase, M., Sakurai, M., Sakai, Y., Tanabe, M. and Mizuno, T. (2024) The Density of CD8(+) Tumor-infiltrating Lymphocytes Correlated With Akt Activation and Ki-67 Index in Canine Soft Tissue Sarcoma. *In Vivo, 38*(4), pp. 1698–1711.

Paget, S. (1989) The distribution of secondary growths in cancer of the breast. 1889. *Cancer Metastasis Rev, 8*(2), pp. 98–101.

Pazdzior-Czapula, K., Otrocka-Domagala, I., Rotkiewicz, T. and Gesek, M. (2014) Cytomorphometry of canine cutaneous histiocytoma. *Pol J Vet Sci, 17*(3), pp. 413–20.

Pegoraro, L., Palumbo, A., Erikson, J., Falda, M., Giovanazzo, B., Emanuel, B. S., Rovera, G., Nowell, P. C. and Croce, C. M. (1984) A 14;18 and an 8;14 chromosome translocation in a cell line derived from an acute B-cell leukemia. *Proc Natl Acad Sci U S A, 81*(22), pp. 7166–70.

Pelletier, J. P., Jovanovic, D. V., Lascau-Coman, V., Fernandes, J. C., Manning, P. T., Connor, J. R., Currie, M. G. and Martel-Pelletier, J. (2000) Selective inhibition of inducible nitric oxide synthase reduces progression of experimental osteoarthritis in vivo: possible link with the reduction in chondrocyte apoptosis and caspase 3 level. *Arthritis Rheum, 43*(6), pp. 1290–9.

Perry, J. A., Culp, W. T., Dailey, D. D., Eickhoff, J. C., Kamstock, D. A. and Thamm, D. H. (2014) Diagnostic accuracy of pre-treatment biopsy for grading soft tissue sarcomas in dogs. *Vet Comp Oncol, 12*(2), pp. 106–13.

Pierezan, F., Mansell, J., Ambrus, A. and Rodrigues Hoffmann, A. (2014) Immunohistochemical expression of ionized calcium binding adapter molecule 1 in cutaneous histiocytic proliferative, neoplastic and inflammatory disorders of dogs and cats. *J Comp Pathol, 151*(4), pp. 347–51.

Pires, I., Alves, A., Queiroga, F. L., Silva, F. and Lopes, C. (2013a) Regression of Canine Cutaneous Histiocytoma: Reduced Proliferation or Increased Apoptosis? *Anticancer Research, 33*, pp. 1397–1400.

Pires, I., Queiroga, F. L., Alves, A., Silva, F. and Lopes, C. (2009) Decrease of E-cadherin expression in canine cutaneous histiocytoma appears to be related to its spontaneous regression. *Anticancer Res, 29*(7), pp. 2713–7.

Pires, I., Rodrigues, P., Alves, A., Queiroga, F. L., Silva, F. and Lopes, C. (2013b) Immunohistochemical and immunoelectron study of major histocompatibility complex class-II antigen in canine cutaneous histiocytoma: its relation to tumor regression. *In Vivo, 27*(2), pp. 257–62.

Prager, I., Liesche, C., van Ooijen, H., Urlaub, D., Verron, Q., Sandstrom, N., Fasbender, F., Claus, M., Eils, R., Beaudouin, J., Onfelt, B. and Watzl, C. (2019) NK cells switch from granzyme B to death receptor-mediated cytotoxicity during serial killing. *J Exp Med, 216*(9), pp. 2113–2127.

Preisler, H. D., Bjornsson, S., Mori, M. and Barcos, M. (1975) Granulocyte differentiation by Friend leukemia cells. *Cell Differ, 4*(5), pp. 273–83.

R Core Team (2019) *R: A Language and Environment for Statistical Computing*, R Foundation for Statistical Computing, Vienna, Austria.

Roberti, M. P., Yonekura, S., Duong, C. P. M., Picard, M., Ferrere, G., Tidjani Alou, M., Rauber, C., Iebba, V., Lehmann, C. H. K., Amon, L., Dudziak, D., Derosa, L., Routy, B., Flament, C., Richard, C., Daillere, R., Fluckiger, A., Van Seuningen, I., Chamaillard, M., Vincent, A., Kourula, S., Opolon, P., Ly, P., Pizzato, E., Becharef, S., Paillet, J., Klein, C., Marliot, F., Pietrantonio, F., Benoist, S., Scoazec, J. Y., Dartigues, P., Hollebecque, A., Malka, D., Pages, F., Galon, J., Gomperts Boneca, I., Lepage, P., Ryffel, B., Raoult, D., Eggermont, A., Vanden Berghe, T., Ghiringhelli, F., Vandenabeele, P., Kroemer, G. and Zitvogel, L. (2020) Chemotherapy-induced ileal crypt apoptosis and the ileal microbiome shape immunosurveillance and prognosis of proximal colon cancer. *Nat Med, 26*(6), pp. 919–931.

Ruterbusch, M., Pruner, K. B., Shehata, L. and Pepper, M. (2020) In Vivo CD4(+) T Cell Differentiation and Function: Revisiting the Th1/Th2 Paradigm. *Annu Rev Immunol, 38*, pp. 705–725.

Santagostino, S. F., Assenmacher, C. A., Tarrant, J. C., Adedeji, A. O. and Radaelli, E. (2021) Mechanisms of Regulated Cell Death: Current Perspectives. *Vet Pathol, 58*(4), pp. 596–623.

Satomi, H., Kobayashi, M., Ito, I., Asano, K., Makino, M., Kawaguchi, K. and Kanno, H. (2025) Predominance of T-bet-positive Th1 cells in infiltrating T-lymphocytes in most of active arteritis lesions of giant cell arteritis. *Virchows Arch, 486*(2), pp. 267–275.

Schlueter, C., Weber, H., Meyer, B., Rogalla, P., Roser, K., Hauke, S. and Bullerdiek, J. (2005) Angiogenetic signaling through hypoxia: HMGB1: an angiogenetic switch molecule. *Am J Pathol, 166*(4), pp. 1259–63.

Schmidt, A. and Weber, O. F. (2006) In memoriam of Rudolf virchow: a historical retrospective including aspects of inflammation, infection and neoplasia. *Contrib Microbiol, 13*, pp. 1–15.

Seung, B. J., Lim, H. Y., Shin, J. I., Kim, H. W., Cho, S. H., Kim, S. H. and Sur, J. H. (2018) CD204-Expressing Tumor-Associated Macrophages Are Associated With Malignant, High-Grade, and Hormone Receptor-Negative Canine Mammary Gland Tumors. *Vet Pathol, 55*(3), pp. 417–424.

Singh, T., Bhattacharya, M., Mavi, A. K., Gulati, A., Rakesh, Sharma, N. K., Gaur, S. and Kumar, U. (2024) Immunogenicity of cancer cells: An overview. *Cell Signal, 113*, pp. 110952.

Smolle, M. A., Herbsthofer, L., Granegger, B., Goda, M., Brcic, I., Bergovec, M., Scheipl, S., Prietl, B., Pichler, M., Gerger, A., Rossmann, C., Riedl, J., Tomberger, M., Lopez-Garcia, P., El-Heliebi, A., Leithner, A., Liegl-Atzwanger, B. and Szkandera, J. (2021) T-regulatory cells predict clinical outcome in soft tissue sarcoma patients: a clinico-pathological study. *Br J Cancer, 125*(5), pp. 717–724.

Snyder, P. W. (2017) Diseases of Immunity. in *Pathologic Basis of Veterinary Disease*. pp. 242–285.e5.

Stanton, S. E. and Disis, M. L. (2016) Clinical significance of tumor-infiltrating lymphocytes in breast cancer. *J Immunother Cancer, 4*, pp. 59.

Steele, K. E., Tan, T. H., Korn, R., Dacosta, K., Brown, C., Kuziora, M., Zimmermann, J., Laffin, B., Widmaier, M., Rognoni, L., Cardenes, R., Schneider, K., Boutrin, A., Martin, P., Zha, J. and Wiestler, T. (2018) Measuring multiple parameters of CD8+ tumor-infiltrating lymphocytes in human cancers by image analysis. *J Immunother Cancer, 6*(1), pp. 20.

Sterenczak, K. A., Kleinschmidt, S., Wefstaedt, P., Eberle, N., Hewicker-Trautwein, M., Bullerdiek, J., Nolte, I. and Murua Escobar, H. (2011) Quantitative PCR and immunohistochemical analyses of HMGB1 and RAGE expression in canine disseminated histiocytic sarcoma (malignant histiocytosis). *Anticancer Res, 31*(5), pp. 1541–8.

Stevenson, V. B., Perry, S. N., Todd, M., Huckle, W. R. and LeRoith, T. (2021) PD-1, PD-L1, and PD-L2 Gene Expression and Tumor Infiltrating Lymphocytes in Canine Melanoma. *Vet Pathol, 58*(4), pp. 692–698.

Stonehewer, J., Simpson, J. W., Else, R. W. and Macintyre, N. (1998) Evaluation of B and T lymphocytes and plasma cells in colonic mucosa from healthy dogs and from dogs with inflammatory bowel disease. *Res Vet Sci, 65*(1), pp. 59–63.

Sur, J. H. (2018) Author Response. *Vet Pathol, 55*(4), pp. 598.

Tang, D., Kang, R., Zeh, H. J. and Lotze, M. T. (2023) The multifunctional protein HMGB1: 50 years of discovery. *Nat Rev Immunol, 23*(12), pp. 824–841.

Taylor, D. O., Dorn, C. R. and Luis, O. H. (1969) Morphologic and biologic characteristics of the canine cutaneous histiocytoma. *Cancer Res, 29*(1), pp. 83–92.

Thomson, D. M. (1975) Soluble tumour-specific antigen and its relationship to tumour growth. *Int J Cancer, 15*(6), pp. 1016–29.

Trojani, M., Contesso, G., Coindre, J. M., Rouesse, J., Bui, N. B., de Mascarel, A., Goussot, J. F., David, M., Bonichon, F. and Lagarde, C. (1984) Soft-tissue sarcomas of adults; study of pathological prognostic variables and definition of a histopathological grading system. *Int J Cancer, 33*(1), pp. 37–42.

Tumeh, P. C., Harview, C. L., Yearley, J. H., Shintaku, I. P., Taylor, E. J., Robert, L., Chmielowski, B., Spasic, M., Henry, G., Ciobanu, V., West, A. N., Carmona, M., Kivork, C., Seja, E., Cherry, G., Gutierrez, A. J., Grogan, T. R., Mateus, C., Tomasic, G., Glaspy, J. A., Emerson, R. O., Robins, H., Pierce, R. H., Elashoff, D. A., Robert, C. and Ribas, A. (2014) PD-1 blockade induces responses by inhibiting adaptive immune resistance. *Nature, 515*(7528), pp. 568–71.

van Smeden, M., Moons, K. G., de Groot, J. A., Collins, G. S., Altman, D. G., Eijkemans, M. J. and Reitsma, J. B. (2019) Sample size for binary logistic prediction models: Beyond events per variable criteria. *Stat Methods Med Res, 28*(8), pp. 2455–2474.

Wickham, H., Averick, M., Bryan, J., Chang, W., McGowan, L., François, R., Grolemund, G., Hayes, A., Henry, L., Hester, J., Kuhn, M., Pedersen, T., Miller, E., Bache, S., Müller, K., Ooms, J., Robinson, D., Seidel, D., Spinu, V., Takahashi, K., Vaughan, D., Wilke, C., Woo, K. and Yutani, H. (2019) Welcome to the Tidyverse. *Journal of Open Source Software, 4*(43).

Willmann, M., Mullauer, L., Guija de Arespacochaga, A., Reifinger, M., Mosberger, I. and Thalhammer, J. G. (2009) Pax5 immunostaining in paraffin-embedded sections of canine non-Hodgkin lymphoma: a novel canine pan pre-B- and B-cell marker. *Vet Immunol Immunopathol, 128*(4), pp. 359–65.

Yang, D., Chen, Q., Yang, H., Tracey, K. J., Bustin, M. and Oppenheim, J. J. (2007) High mobility group box-1 protein induces the migration and activation of human dendritic cells and acts as an alarmin. *J Leukoc Biol, 81*(1), pp. 59–66.

Yap, F. W., Rasotto, R., Priestnall, S. L., Parsons, K. J. and Stewart, J. (2017) Intra- and inter-observer agreement in histological assessment of canine soft tissue sarcoma. *Vet Comp Oncol, 15*(4), pp. 1553–1557.

Yatim, N., Cullen, S. and Albert, M. L. (2017) Dying cells actively regulate adaptive immune responses. *Nat Rev Immunol, 17*(4), pp. 262–275.

Yuan, J. and Ofengeim, D. (2024) A guide to cell death pathways. *Nat Rev Mol Cell Biol, 25*(5), pp. 379–395.

Zhang, C., Yang, M. and Ericsson, A. C. (2021) Function of Macrophages in Disease: Current Understanding on Molecular Mechanisms. *Front Immunol, 12*, pp. 620510.

Zheng, X., Weigert, A., Reu, S., Guenther, S., Mansouri, S., Bassaly, B., Gattenlohner, S., Grimminger, F., Pullamsetti, S., Seeger, W., Winter, H. and Savai, R. (2020) Spatial Density and Distribution of Tumor-Associated Macrophages Predict Survival in Non-Small Cell Lung Carcinoma. *Cancer Res, 80*(20), pp. 4414–4425.